Disturbance growth in a laminar separation bubble subjected to free-stream turbulence

Tomek Jaroslawski, Maxime Forte, Olivier Vermeersch, Jean-Marc Moschetta, Erwin Gowree

Disturbance growth in a laminar separation bubble subjected to freestream turbulence

Tomek Jaroslawski[1] †, Maxime Forte[1], Olivier Vermeersch[1], Jean-Marc Moschetta[2] and Erwin R. Gowree[2]

[1]ONERA, DMPE, Universite de Toulouse, 31055, Toulouse, France.

[2]ISAE-SUPAERO, Universite de Toulouse, 31055, Toulouse, France.

(Received xx; revised xx; accepted xx)

Experiments were conducted to study the transition and flow development in a laminar separation bubble (LSB) formed on an aerofoil. The effects of a wide range of freestream turbulence intensity ($0.15\% < Tu < 6.26\%$) and streamwise integral length scale ($4.6mm < \Lambda_u < 17.2mm$) are considered. The co-existence of modal instability due to the laminar separation bubble (LSB) and non-modal instability caused by streaks generated by freestream turbulence is observed. The flow field is measured using hotwire anemometry, which showed that the presence of streaks in the boundary layer modifies the mean flow topology of the bubble. These changes in the mean flow field result in the modification of the convective disturbance growth, where an increase in turbulence intensity is found to dampen the growth of the modal instability. For a relatively fixed level of Tu, the variation of Λ_u has modest effects. However, a slight advancement of the non-linear growth of disturbances and eventual breakdown with the decrease in Λ_u is observed. The data shows that the streamwise growth of the disturbance energy is exponential for the lowest levels of freestream turbulence and gradually becomes algebraic as the level of freestream turbulence increases. Once a critical turbulence intensity is reached, there is enough energy in the boundary layer to suppress the laminar separation bubble, resulting in the non-modal instability taking over the transition process. Linear stability analysis is conducted in the fore position of the LSB. It accurately models incipient disturbance growth, unstable frequencies and eigenfunctions for configurations subjected to turbulence intensity levels up to 3%, showing that the mean flow modification due to the non-modal instability dampens the modal instability.

Key words: /

1. Introduction

At low Reynolds numbers ($Re < 5 \times 10^5$, based on the chord of the aerofoil and the freestream velocity, $Re = U_\infty c/\nu$) viscous effects are so significant, such that the presence of a strong enough adverse pressure gradient can cause a laminar boundary layer to separate from the wall. These flows occur in many engineering applications such as low-pressure

† Email address for correspondence: thomas.jaroslawski@onera.fr

turbines (Volino 1997) and micro-aerial vehicles (Jaroslawski *et al.* 2022). As a result of boundary layer separation, a laminar shear layer undergoes transition to turbulence, negatively impacting the noise emissions, lift, drag and unsteady loading of the aerodynamic surface (Carmichael 1981).

In a time-averaged sense, depending on the Reynolds number, angle of incidence and the amount of freestream disturbance, the separated shear layer will remain separated or reattach to the wall. Gaster (1967) proposed a two-parameter criterion, considering a pressure gradient parameter and a Reynolds number based on the momentum thickness at separation ($Re_{\delta_{2,sep}} = U_\infty \delta_{2,sep}/\nu$). For weakly adverse pressure gradients and high values of $Re_{\delta_{2,sep}}$, the separated shear layer will reattach as a turbulent boundary layer, forming a closed region of recirculating fluid, commonly referred to as a laminar separation bubble (LSB) or "short bubble". With an increase in incidence or decrease in $Re_{\delta_{2,sep}}$, the separated shear layer may fail to reattach, and the "short bubble" may burst to form either a "long bubble" or an unattached free shear layer. In a low freestream disturbance environment, the mechanisms of boundary layer transition in the separated shear layer are through the amplification of low-amplitude disturbances, where Diwan & Ramesh (2009) provided evidence that the origin of the inflectional instability in an LSB can be traced back to a region upstream of separation where the disturbances in the attached boundary layer are amplified through a viscous instability. Xu *et al.* (2017) showed similar behaviour in 3D confined separation bubbles, where the disturbance growth was strongly dependent on the initial disturbance, similarly to what was postulated by Diwan & Ramesh (2009), where the former's DNS showed that the transition to turbulence would not occur without the presence of excitation, despite the base flow being highly inflected. The transition process in the separated shear layer involves the primary amplification of perturbations. It is credited to an invicsid Kelvin-Helmholtz (KH) instability in the fore portion of the bubble, which is modelled well with Linear Stability Theory (LST) (Rist & Maucher 2002; Marxen *et al.* 2003; Häggmark *et al.* 2001; Kurelek *et al.* 2018; Yarusevych & Kotsonis 2017). Rist & Maucher (2002) demonstrated that the wall-normal distance and intensity of the separated shear, maximum reverse flow and Reynolds number are critical parameters governing the stability of the bubble. Moreover, they showed that if the wall-normal distance of the separated shear layer or the reverse flow in the bubble is large enough (15-20% of the freestream velocity), a global instability can be triggered within the bubble. More recently, Rodriguez & Theofilis (2010),Rodríguez & Gennaro (2019) and Rodríguez *et al.* (2021) showed it could occur at even lower reverse flow velocities (7% of the freestream velocity). Finally, global instabilities stem from numerical investigations conducted in environments with zero freestream turbulence, so their relevance in experiments remains to be determined.

In boundary layer flows subjected to no pressure gradient, laminar to turbulent transition induced by freestream turbulence (FST) follows a different transition mechanism than classical modal theory and is often referred to as "bypass" transition, which was first used by Morkovin (1985), referring to the bypassing of the current knowledge of the transition mechanisms which was limited to modal theory at the time. However, since then, substantial efforts have been made to understand the transition process in wall-bounded flows subjected to freestream turbulence. Klebanoff & Tidstrom (1972) brought the first physical understanding of transition induced by FST, where the presence of three-dimensional (3D) low-frequency fluctuations inside the laminar boundary layer lead to fluctuations in the boundary layer thickness, often thought of as thickening and thinning of the boundary layer. This distortion of the boundary layer is dominated by streamwise velocity fluctuations, resulting in longitudinal streaks. When the FST level is greater than 1%, the unsteady streamwise streaks (known as Klebanoff modes) dominate the transition process, occurring at low frequencies (Arnal & Julien 1978) and having disturbance levels up to 10% of the freestream velocity (Westin

et al. 1993). Streaks or Klebanoff modes form, through the "lift-up" mechanism, consisting of energy transfer between the wall-normal velocity fluctuations (v') and the streamwise velocity fluctuations (u'), resulting in the streamwise non-modal growth of disturbances inside the boundary layer (Brandt *et al.* 2004; Volino 1997; Nolan *et al.* 2010; Andersson *et al.* 1999; Luchini 2000). Consequently, the maximum value of the streamwise perturbation along the wall-normal direction occurs at a location corresponding to the middle of the boundary layer (Arnal & Julien 1978), in contrast to the near wall location in natural/modal transition, and was later theoretically explained by optimal perturbation theory (Andersson *et al.* 1999; Luchini 2000).

In transition experiments, freestream turbulence is often generated by static uniform grids, where the growth of disturbances in the boundary layer is highly dependent on the turbulence generating grid (Westin *et al.* 1993; Kendall 1998). The integral length scale, which generally scales by the mesh size, M, can be considered the average energy-containing vortex's size and is an important parameter when investigating the mechanisms present in transition induced by freestream turbulence. Hislop (1940) demonstrated that the integral length-scale partially influenced the location of transition, reporting that the transition position would move downstream as the streamwise integral length scale (Λ_u) increased. In contrast, to the results first proposed by Hislop (1940), Jonáš *et al.* (2000) and Brandt *et al.* (2004) demonstrated that the transition position moves upstream with an increase of Λ_u. More recently, based on a set of 42 grid configurations, Fransson & Shahinfar (2020) created a semi-empirical transition prediction model considering Λ_u and Tu at the leading edge. It was hypothesised that there exists an optimum ratio between the boundary layer thickness (δ) and Λ_u, which promotes transition, stating that an increase in Λ_u would move the transition location upstream when $\Lambda_u < 3\delta$, and $vice\ versa$. In general, they concluded that for low Tu, the increase in Λ_u will advance the transition position and that for high levels of Tu, an increase in Λ_u would delay transition, and was recently confirmed with further experiments by Mamidala *et al.* (2022). Moreover, flat plate experiments by Fransson *et al.* (2005) (leading edge FST level: $1.4\% < Tu < 6.7\%$) found that the disturbance energy is proportional to $Tu^2 Re_x$, (Tu denotes the freestream turbulence intensity and Re_x, the Reynolds number based on the freestream velocity and streamwise distance from the leading edge) verifying theoretical non-modal growth predictions proposed by Andersson *et al.* (1999) and Luchini (2000). The complexity of freestream turbulence-induced boundary layer transition stems from the boundary layer thickness growing with the downstream distance. Since the FST decays and the integral length scales grow in the streamwise direction, the forcing on the boundary layer changes gradually in the streamwise direction.

The effects of freestream turbulence and integral length scale on boundary layer transition in LSBs have not been addressed to the same extent as for attached boundary layers; notably, there is a lack of experimental results and the role of the integral length scales. Häggmark *et al.* (2000) provided some of the first experimental results on the effects of grid-generated FST (with levels of 1.5% at the leading edge) on an LSB generated over a flat plate subjected to an adverse pressure gradient using hot wire anemometry measurements. They found low-frequency streaky structures in the boundary layer upstream of the separation and in the separated shear layer from smoke visualisation and spectral analysis. No strong evidence for the existence of 2D waves, which are typical for separation bubbles in an undisturbed environment, were found. More recently, Istvan & Yarusevych (2018) experimentally investigated the effects of FST (regular static grid, $Tu = 0.06\%$ to 1.99%) on an LSB formed over a NACA0018 aerofoil for chord-based Reynolds numbers of 80000 and 150000 using Particle Image Velocimetry (PIV). They found that the bubble was highly sensitive to FST, and increasing the level leads to a thinner bubble and a decrease in its chordwise length due to a downstream shift of the separation point and an upstream shift

of the reattachment point as in past experimental works (Burgmann & Schröder 2008; Olson *et al.* 2013).Istvan & Yarusevych (2018) concluded that the maximum spatial amplification of disturbances in the separated shear layer decreased with the increase in Tu, implying that the larger initial disturbances are solely responsible for the earlier transition and reattachment. At levels of FST of 1.99%, streamwise streaks were qualitatively observed upstream and inside the bubble, signifying the onset of turbulence induced or "bypass" transition. Simoni *et al.* (2017) used PIV to characterise the effects of Reynolds number (40000 to 90000) and FST (Tu = 0.65% to 2.87%) on an LSB generated over a flat plate, finding similar trends as Istvan & Yarusevych (2018). Moreover, Dellacasagrande *et al.* (2020) generated an empirical correlation for the transition onset Reynolds number based on pressure gradient and Tu. They hypothesised that the Reynolds number variation mainly drives the length scale associated with the KH vortices and inline with Burgmann & Schröder (2008), whereas increasing the intensity of the FST level shifts the onset of the shedding phenomenon upstream.

In LSBs subjected to sufficient levels of FST, the co-existence between modal and non-modal instabilities arise. Hosseinverdi & Fasel (2019) used direct numerical simulations (DNS) to investigate the role of isotropic FST (with intensities of 0.1% to 3%) on the hydrodynamic instability mechanisms of an LSB. They reported that the FST induced Klebanoff modes (streaks) upstream of the separation location, proposing that the boundary layer transition process was made up of two mechanisms. The first consisted of low-frequency Klebanoff modes (streaks) induced by the FST, and the second was a KH instability enhanced by the FST. Depending on the level of FST, either one or both of these mechanisms would dominate the transition process. They found that the KH instability was triggered much earlier, and transition was enhanced, leading to a drastic reduction in the size of the separation bubble. The streamwise streaks (Klebanoff modes) prior to the separation location led to a faster breakdown of the KH vortices. They concluded that the energy carried by the Klebanoff modes increased with the Tu, thus leading to a more significant reduction in the mean separated region. Other DNS studies by Wissink & Rodi (2006) (flat plate, counter form wall to for pressure gradient and with a leading edge Tu = %1.5) showed that the nature of the instability mechanisms changes from modal amplification due to the KH instability to amplification of streamwise streaks for elevated levels of FST. These streaks extend into the region of the laminar separated flow and initiate breakdown via the formation of turbulent spots. Balzer & Fasel (2016) showed that even minimal FST levels caused a significant reduction of the separation bubble size, indicating a strong effect of Tu on transitional LSBs and found that elevated FST levels led to the formation of streaks. They also observed that the inviscid shear-layer instability was present even for levels of turbulence intensity of 2.5%, concluding that the transition to turbulence was a consequence of both the primary shear-layer instability and the enhanced 3D disturbance level, in particular the streamwise streaks caused by the FST. A recent LES investigation by Li & Yang (2019) on a low-pressure turbine blade subjected to a leading edge turbulence intensity level of Tu = 2.9%, suggested that the secondary instability breaking down into three-dimensional structures is "bypassed" due to the high levels of FST.

The role of the integral length scale on the boundary layer transition mechanisms in an LSB is seldom studied due to the experimental difficulty of controlling this parameter. However, numerical studies by Hosseinverdi & Fasel (2019) have shown that a freestream turbulence level between $Tu = 0.1 - 2\%$ and varying the integral length scale from $0.9\delta_1 - 3\delta_1$ had minimal effects on the mean bubble size. Breuer (2018) conducted Large Eddy Simulations (LES) on an aerofoil subjected to FST, finding that a decrease in the integral length scale advanced the transition position, which was attributed to the fact that the smaller scales could penetrate the shear layer more easily than larger scales, effectively increasing the receptivity.

The present work investigates the effects of forcing a laminar separation bubble with

an extensive range of Tu and Λ_u on the flow development, stability and transition of the bubble. Freestream turbulence is generated, in a controlled manner, using a variety of regular and fractal grids set up so that turbulence interacting with the bubble would be approximately isotropic and homogeneous. The aim is to investigate, experimentally, the co-existence of modal and non-modal growth of disturbances in the laminar separation bubble, their interaction and their effects on the transition process. The flow field developing over a two-dimensional aerofoil is measured using hotwire anemometry. Infra-red thermography measurements and integral boundary layer calculations are used to validate the baseline flow configuration. The freestream turbulence is characterised in detail using a two-component hotwire anemometer, before the leading edge and above the flow developing over the aerofoil, where the turbulence intensity, integral length scale and spectra are analysed. The detailed measurements of boundary layer development allow the characterisation of the disturbance growth mechanisms inside the bubble and are accompanied by a linear stability analysis which model the convective growth of modal disturbances inside the bubble subjected to elevated levels of freestream turbulence.

2. Experiments

2.1. *Wind tunnel setup*

The experiments were conducted at atmospheric conditions in the ONERA Toulouse TRIN 2 subsonic wind tunnel. The wind tunnel has a contraction ratio of 16 and a test section entrance dimensions of 0.3 m width × 0.4 m height and a total length of 2 m. The flow exits the test section through a diverging nozzle with an expansion ratio of 3. It is discharged through a noise reduction chamber, which aims to prevent pressure waves from the exit driving fan downstream from propagating upstream into the test section and possibly interfering with the receptivity of the aerofoil. As a result, the maximum freestream turbulence level (measured near the leading edge of the aerofoil, cf. Fig. 1) in the test section with the aerofoil mounted was found to be below 0.15 % and is calculated by the integral of the power spectral density of the velocity signal over frequencies ranging from 3Hz to 10 kHz. All experiments were conducted on an aluminium NACA 0015 aerofoil model from Studer *et al.* (2006), who demonstrated that the model mounted in the TRIN2 wind tunnel exhibited a bi-dimensional flow in the region of interest of the current experiments; without the use of any flow control strategies. The model was mounted horizontally in the test section with the leading edge placed 1.44 m downstream of the test section inlet and had a chord length (c) and span of 0.3 and 0.4 m, respectively. The freestream velocity was fixed at $U_\infty \cong 6m/s$ for all test configurations, corresponding to a chord based Reynolds number, $Re_c = U_\infty c/\nu$ of 125000. The angle of attack, AoA, was fixed to the same value throughout all experiments. An AoA of 2.3° was used as it allowed the traversing system to access all positions in the bubble while keeping the blockage ratio in the tunnel low. The experimental setup is presented in Fig. 1. Finally, it is important to note that the current experimental setup did not allow for spanwise measurements.

2.2. *Boundary layer and freestream flow measurements*

Velocity measurements are acquired using a hotwire probe mounted on a two-dimensional traverse. The probe's position in the streamwise, x, and wall-normal, y, directions is measured using Heidenhain LS388 linear encoders, with a stepping accuracy of $5\mu m$. Boundary layer measurements were made using constant temperature hotwire anemometry (HWA) using a Dantec Dynamics Streamline Pro system with a 90C10 module and a 55P15 boundary layer probe. To accurately evaluate the distance between the measurement probe and the

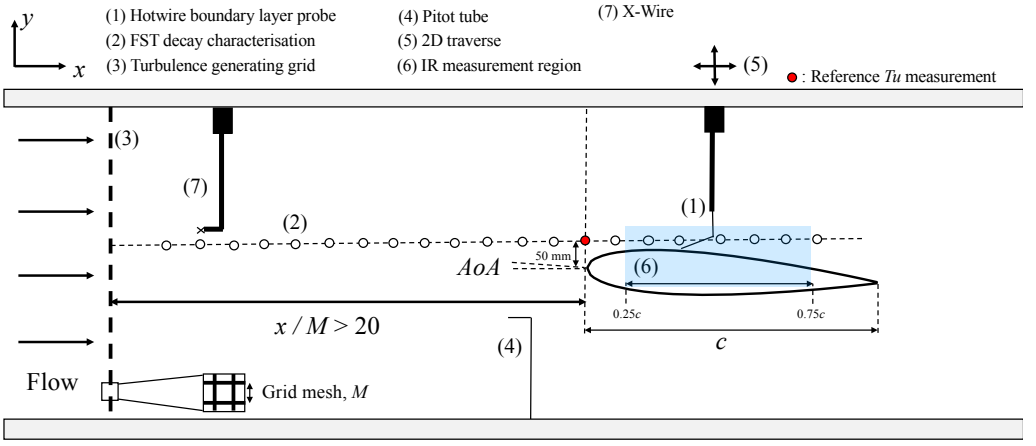

Figure 1: Experimental Setup. NB: The reference turbulence intensity level and integral length scale are taken at the Tu reference measurement location (red marker), which are used to characterise each configuration for this study.

wall, a camera equipped with a SIGMA 180 mm 1:3:5 APO-MACRO-DG-HSM-D lens and a 2× SIGMA EX teleconverter is used to set the zero for each boundary layer profile measurement, where the closest measurements to the wall are taken at 200 μm, to avoid any near wall correction, due to thermal effects between the wall and the hotwire. The effect of tripping on the pressure side of the aerofoil was verified, with no significant effects found on the mean flow, unstable frequencies in the boundary layer and shedding frequency of the aerofoil. This observation suggests that at the trailing edge of the pressure side of the aerofoil, the boundary layer is attached and turbulent. Freestream turbulence measurements were conducted using a 5 μm Dantec 55P51 probe, where a 6 mm diameter Dantec 55H24 support was used to support the X-wire probes. All test data were acquired using a National Instruments CompactDAQ-9178 with two NI-9239 (built-in resolution of 24 bit) modules for voltage measurements and a NI-9211 (built-in resolution of 16 bit) module for temperature measurements. Both single- and X-probes were calibrated $in-situ$ against a pitot tube connected to an MKS 220DD pressure transducer. The boundary layer probe (55P15) was calibrated using King's law (Bruun 1996) and the zero velocity voltage in the calibration was taken as the absolute minimum voltage measured over the sample duration with the wind tunnel off (Watmuff 1999). The X-wires (55P51) were calibrated for a velocity range of approximately 3 - 12 m/s and nine angles ranging between $-28°$ to $+28°$. The velocities were obtained using the look-up table approach described by Burattini & Antonia (2005) and Lueptow *et al.* (2004). Hotwire drift was accounted for by conducting pre-and post-experiment calibrations. The frequency response of the system was estimated using the standard pulse-response test. It was approximately 45 kHz, well above these experiments' spectral region of interest. The sampling frequency f_s was set to $f_s = 2f_c + 500$ Hz, where the f_c is the cutoff frequency, in the present work $f_s = 25$ kHz, and sampling time was set so that second-order statistics would converged to at least ±1% at every location using the 95% confidence interval (Benedict & Gould 1996). This resulted in mean profile measurements being conducted for 10 seconds for each point. The freestream turbulence generated by the grids was characterised using the X-probe. Streamwise measurements were taken along the wind tunnel's centre line before the aerofoil's leading edge and 20mm above the surface of the aerofoil. A stabilisation time of 10 seconds was used between traverse movements to ensure any vibrations from the movement had dampened out. It should be noted that the purpose of

this study was not a detailed investigation into the mechanisms of the decay of grid-generated turbulence. However, some care was taken in ensuring at least 40000-60000 integral lengths of the flow were measured (corresponding to about a sampling time of 120 seconds for each point) to obtain accurate converged statistics when characterising the freestream turbulence generated by the grids. The uncertainty in hotwire measurements was estimated to be less than 3%, for $U/U_\infty > 0.2$ and the uncertainty in the hotwire positioning is estimated to be less than 0.05 mm. The use of HWA in the study of LSBs is fraught with difficulty. In particular, the mean velocity measurement cannot detect the reverse flow region in the LSB. Furthermore, fluctuating velocity measurements are limited due to a non-negligible normal or spanwise component; however, it is not an issue for the amplification growth rate as the maximum value of fluctuations is outside the separated region. Nevertheless, as demonstrated by Boutilier & Yarusevych (2012), HWA can be used to study the transition mechanisms in an LSB. Spanwise measurements were not possible due to limitations in the experimental setup. The impact of forcing on the bubble's wall-normal height would modify the modal instability mechanism in a separated boundary-layer profile. The eigenfunctions can recover features of both Tollmien-Schlichting and Kelvin-Helmholtz instabilities where the height of the bubble is related to which amplifying mechanism dominates the transition process (Rist & Maucher 2002).

2.3. *Characterisation of freestream turbulence*

The freestream turbulence is characterised by its intensity (Tu and Tv) and streamwise and vertical integral length scales (Λ_u and Λ_v, respectively). The integral length scale is the most energetic scale, corresponding to the average energy-containing vortex's average size. Other scales of turbulence consist of the Kolmogorov, the smallest viscous scale and the Taylor length scale, the smallest energetic length scale in the turbulent flow and are not believed to be important scales for the boundary layer transition process (Fransson & Shahinfar 2020). Freestream turbulence was generated using a variety of static turbulence generating grids. Different grid solidities(σ), mesh sizes (M), bar thickness (t) and relative distances between the grid and the leading edge can be used to vary the FST characteristics. In the present work, the values of σ were kept within limits recommended by Kurian & Fransson (2009), and M was varied to change the levels of turbulence intensity. Placing the grid closer to the leading edge leads to a lower integral length scale and high turbulence intensity (Tu). The difficulty of keeping the FST level fixed while varying the scale was highlighted by Fransson & Shahinfar (2020). Generally, the FST length scales are functions of M and t of the grid and the turbulence intensity by the σ (proprietorial to the pressure drop). The streamwise position of the grids (for grids with $M = 6$ and 12 mm) is varied to change the value of the integral length scale while keeping the value of Tu relatively constant, a similar method has been used by Jonáš *et al.* (2000) and Fransson & Shahinfar (2020). All grids were placed at least $20M$ away from the leading edge of the aerofoil, ensuring the FST is relatively isotropic and homogeneous. The Tu and Tv is defined in Eq. 2.1.

$$Tu = \frac{u_{rms}}{U_\infty}, Tv = \frac{v_{rms}}{U_\infty} \tag{2.1}$$

The Λ_u and Λ_v are calculated by integrating the autocorrelation of their fluctuating velocity signals and applying Taylor's hypothesis of frozen turbulence, which converts the time to spatial scales, and is presented in Eq. 2.2:

$$\Lambda_{u,v} = U_\infty \int_0^\infty f(\tau) d\tau \tag{2.2}$$

Grid Type.	$M(mm)$	σ	$t(mm)$
Regular	3	36	0.6
Regular	6	31	1
Regular	12	44	3
Regular	50	33	9
Regular	70	36	14
Fractal	140	28	13

Table 1: Parameters of turbulence generating grids. NB: The fractal grid is characterised by the size of the largest element, M_f.

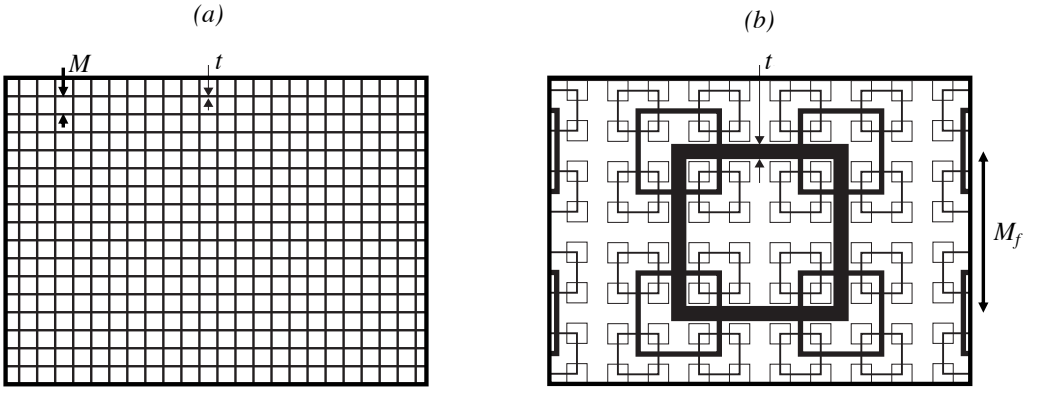

Figure 2: Schematics of grids used. (a) Regular grid (configs. C0-C6) and (b) fractal grid (config. C7)

where $f(\tau)$ denotes auto-correlation function of the signal and τ the time delay. The auto-correlation function was numerically integrated until the first zero crossing to obtain the integral length scale (Kurian & Fransson 2009). Experimental investigations of boundary layer transition induced by freestream turbulence have used active grids to generate larger values of turbulence intensity, and Λ_u such as in Makita & Sassa (1991); Fransson *et al.* (2005). The experimental implementation of this grids is costly, hence in the present work, a fractal grid was leveraged to generate high levels of turbulence intensity and length scales of turbulence under the condition that the grid is sufficiently far away from the leading edge such that the flow is more spatially homogeneous (Hurst & Vassilicos 2007). The present work does not consider investigations of the effects of non-equilibrium turbulence near the fractal grid. A summary of the grids tested in the current work can be found in Table 1, with the schematics of the regular and fractal grids presented in Fig. 2.

The turbulence parameters relevant to the current investigation are summarised in Table 2. The decay and evolution of the turbulence level, *Tu*, *Tv* and its integral length scales, Λ_u, Λ_v are presented in Fig. 3a,b and Fig. 3c,d, respectfully. In agreement with previous studies, from Fig. 3a,b exponential decay of *Tu* and *Tv* is present before the leading edge of the aerofoil, and the integral length scales increase in size moving further away from the grid. The development of the FST over the aerofoil shows that the *Tu* is rather constant over the entire aerofoil, except for the highest *Tu* configurations where it still decreases near the leading edge. In zero pressure gradient boundary layers subjected to freestream turbulence, the *Tu* continues to decay in the streamwise direction (Fransson *et al.* 2005; Brandt *et al.*

Config.	v_{rms}/u_{rms}	$Tu(\%)$	$\Lambda_u(mm)$	$\Lambda_v(mm)$	x/M
NG	0.92	0.15	210	181	-
C0	0.82	0.64	4.6	3.1	480
C1	0.91	1.21	8.7	5.5	143
C2	0.81	1.23	10.3	6.7	240
C3	0.92	1.31	8.3	5.6	138
C4	1.07	1.63	12.3	8.3	120
C5	1.07	2.97	15.4	10.6	29
C6	1.02	4.16	16.8	11.4	21
C7	1.10	6.26	17.2	13.3	-

Table 2: Freestream turbulence test matrix. Turbulence isotropy, turbulence intensity (*Tu*), streamwise and vertical integral length scale (Λ_u and Λ_v, respectively) at the leading edge of the aerofoil ($x/c = 0$). NB. Λ_u and Λ_v are presented for the NG configuration for completeness, and are a result of the low disturbance flow, where the large length scales reflect a small perturbation to the mean flow.

2004; Jonáš *et al.* 2000) which is not the case in the present work as the favourable pressure gradient near the leading edge of the aerofoil could be responsible for this behaviour. From Fig.3b, it can be seen that for configurations C1, C2 and C3, the *Tu* is relatively constant at the leading edge of the aerofoil with the integral length scales varying from 8.3 - 10.3 mm. The slight increase of the integral length scales after the leading edge could be due to the increased velocity near the leading edge of the aerofoil. This could suggest that the freestream forcing on the boundary layer behaves differently in the present configuration (aerofoil) than for a flat plate with zero pressure gradient; however, this is out of the scope of this present work and has been recently investigated experimentally by Mamidala *et al.* (2022). Nevertheless, the current experimental characterisation of the freestream turbulence behaviour before and around the aerofoil can serve as an input for future numerical studies. The power spectral density (PSD) of the FST is presented in Fig.4, the inertial sub-range is largest for the configurations with the largest levels of *Tu*, coherent with the values of Λ_u and Λ_v.

3. Results

The results presented here pertain to experiments conducted on a NACA 0015 aerofoil at an angle of attack of 2.3° and Re_c of 125000. For these conditions, the effects of FST and integral length scale on the transition process in an LSB are considered. The time averaged flow is presented in Sec. 3.1 followed by an unsteady analysis, instability and disturbance growth investigation in 3.2.

3.1. *Time-averaged flow field*

3.1.1. *Baseline LSB*

Mean surface pressure measurements were conducted; however, the spacing of the pressure taps was too large to determine the streamwise positions of mean separation (x_S), transition (x_T) and reattachment (x_R). Consequently, HWA/IRT measurements and numerical calculations were employed to characterise the baseline configuration. Measured boundary layer profiles before x_S were independently validated using ONERA's in-house boundary layer code 3C3D, which solves Prandtl's equations for three-dimensional boundary layers using a method of characteristics along local streamlines. The boundary layer equations were set up

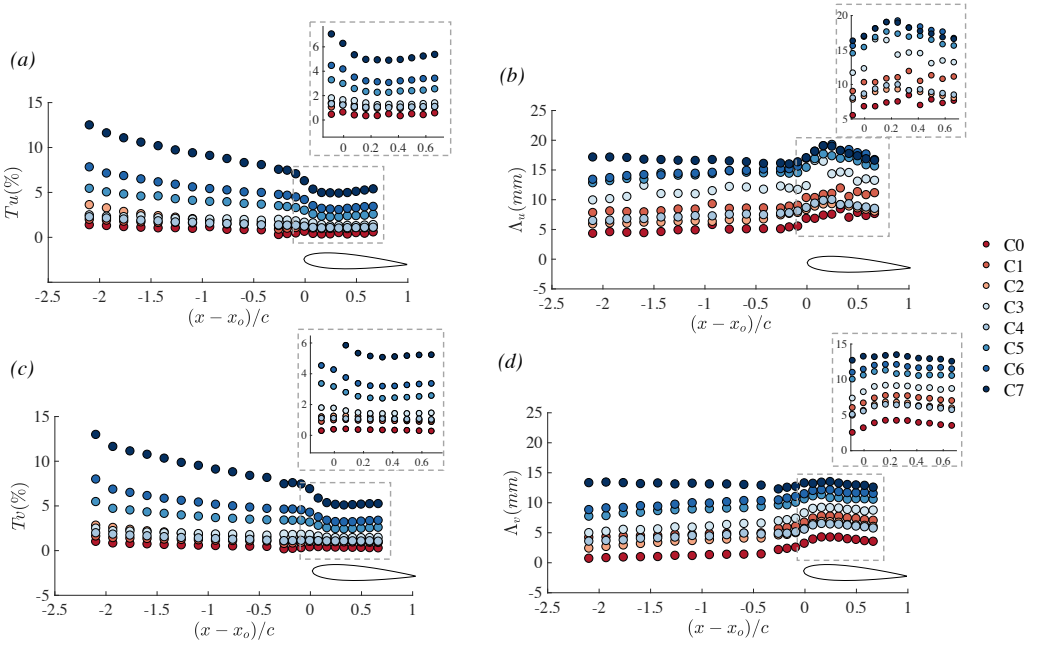

Figure 3: Streamwise evolution of Tu (a), Λ_u (b), Tv (c) and Λ_v (d) for freestream turbulence configurations C0-C7

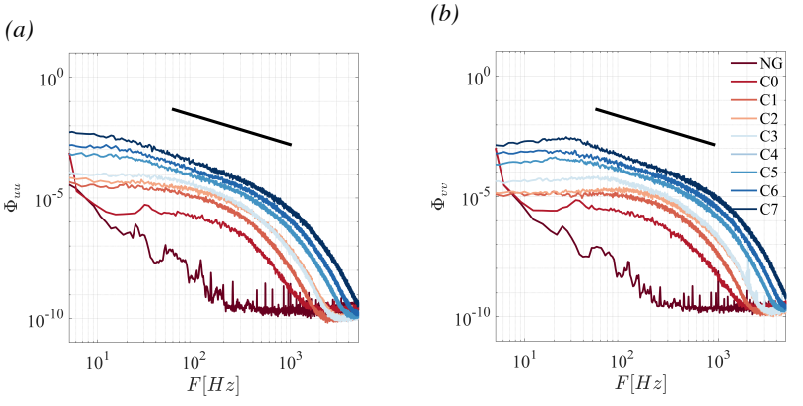

Figure 4: Power Spectral Density ($\Phi_{xx}[m^2/s^2]$) at the leading edge ($x/c = 0$) of the aerofoil. (a) Power Spectral Density for u' (Φ_{uu}) and (b) Power Spectral Density for v' (Φ_{vv}) .

using a body-fitted coordinate system, and the momentum equations are discretised along the local streamlines (Houdeville 1992). The streamwise pressure distribution serves as an input to the boundary layer calculations. The interpolated measured pressure distribution and a numerical pressure distribution calculated with XFOIL (critical amplification factor, $N_{crit} = 6$) (Drela 1989) were used and found to yield close results. Referring to Fig. 5a, laminar boundary layer profile development can be observed upstream of the separation point, with results from the experiment and the boundary-layer solver having a difference in 7% in the chordwise evolution of the integral parameters. The boundary-layer solver stops the calculations at $x = 0.394c$ since no model for separated flows is implemented into

the solver and corresponds to approximately x_S. Mean velocity profiles downstream of the separation point (Fig. 5b) exhibit reverse flow (although cannot be directly measured with HWA) near the wall and a profile inflection point at a vertical distance corresponding to the displacement thickness (δ_1), with the flow, eventually reattaching as a turbulent boundary layer (cf. $x = 0.7c$, Fig. 5b). Moreover, relevant to linear stability (LST) calculations, the errors in mean velocity profiles, especially on those after separation and in the flow reversal region, have only a minor effect on the linear stability predictions of disturbance growth rates (Boutilier & Yarusevych 2012).

The exact position of the separation is not critical for this study as the focus is the instability characteristics, however as a good experimental practice, it was characterised by the limits of the experimental setup which would be important for future numerical simulations. From HWA measurements, x_S is obtained by assuming that boundary layer separation occurs where $\partial u/\partial y = 0$, near the wall. In the present results, this location is determined to be $0.375c$, which agrees with that obtained from 3C3D, considering the spatial resolution of the HWA measurements would introduce an uncertainty of approximately $\pm 0.025c$. The experimental determination of x_S is often fraught with difficulty, as demonstrated by Istvan & Yarusevych (2018), who were able to determine the x_S with an uncertainty ranging from $0.125c$ to $0.2c$ and Simoni *et al.* (2017) were not able to distinguish a difference in the separation position for different Reynolds numbers and FST configurations. For this reason, separate infrared thermography (IRT) measurements (not presented here) found that that separation occurs at approximately $0.36c$. The objective of this study is to investigate the disturbance growth and how FST impacts the transition mechanisms in the separated shear layer; therefore, the current accuracy x_S is sufficient. Considering the different values of x_s obtained from HWA, IRT and the boundary-layer solver have a standard deviation of $0.02c$, considering the measurement resolution error in the HWA measurements, the approximate uncertainty of x_s is $0.07c$.

The mean streamwise velocity contour in Fig. 6a,b show the presence of a mean LSB that extends from $x_S/c = 0.375 \pm 0.07$ until $x_R/c = 0.700 \pm 0.025$. The bubble reaches its maximum height (x_H) at $x/c = 0.575 \pm 0.025$, where reasonable agreement has been found between maximum bubble height and mean transition position in previous work (Kurelek *et al.* 2018; Yarusevych & Kotsonis 2017), and will be used to define x_T for configurations with an LSB in the present work. Additionally, although not presented here, IRT measurements identified a transition close to what corresponds to the maximum bubble height from the hotwire measurements.

The streamwise unfiltered root-mean-square (r.m.s) velocity field in Fig. 6b and profiles in the wall-normal direction in Fig.5 show a gradual streamwise development of the fluctuations in the attached laminar boundary layer with a single peak near the wall emerging before the separation point suggesting a viscous instability which has been sufficiently amplified to be detected by the measurement probe. Downstream, in the separated flow region, the spatial amplification of fluctuations increases rapidly in the laminar separation bubble, with a maximum at approximately $y/\delta_1 \approx 1$, which is in the vicinity of the inflexion point. The u_{rms} profiles in the wall-normal direction exhibit a multiple peak pattern inside the bubble, agreeing with Rist & Maucher (2002) specifically just upstream of the reattachment position, showing the amplification of two near wall peaks at $y/\delta_1 \approx 0.2 - 0.5$ and 1 (cf. Fig 5). This indicates the growth of disturbances in the reserve flow region and separated shear layer with the latter following the displacement thickness (Kurelek *et al.* 2018). Qualitatively, the streamwise u_{rms} profiles are similar to the velocity fluctuation profile predicted by LST (Rist & Maucher 2002), indicating the modal decomposition of these profiles could yield meaningful comparisons with LST. Moreover, u_{rms} profiles have a single peak near the wall (cf. Fig. 5 at $x/c = 0.7$) and diminish more gradually into the freestream than in the

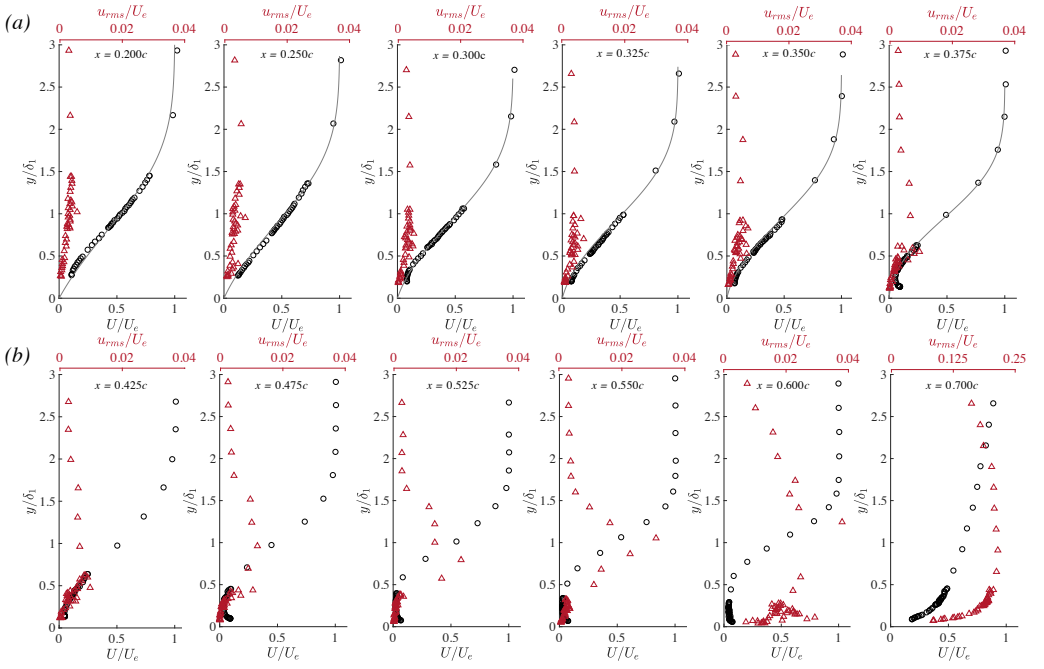

Figure 5: (a) streamwise evolution of streamwise velocity (U) profiles (black) and unfiltered u_{rms} profiles before the separation position (x_s) where markers represent experimental measurements and the black lines represents results obtained from 3C3D and (b) after x_s ($x = 0.394c$) and until the reattachment position x_R. NB: The wall-normal distance of each proifle is scaled with the local value of δ_1.

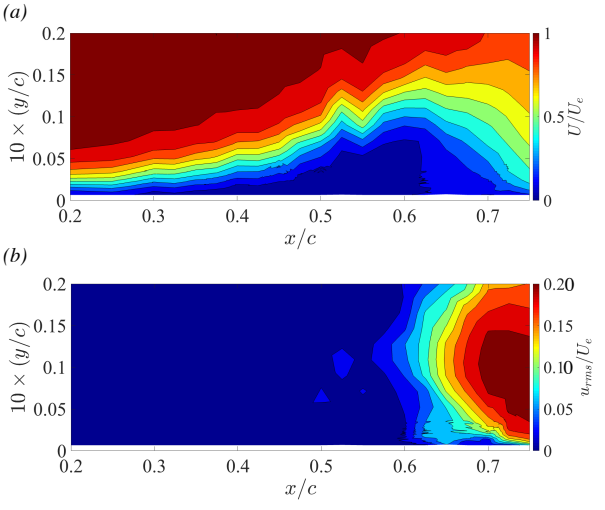

Figure 6: Contours (21 velocity profiles) of (a) the mean streamwise velocity (U) and (b) the r.m.s of the fluctuating streamwise velocity (u_{rms}).

414 attached laminar boundary layer upstream, which is expected for a turbulent boundary and
415 in agreement with previous results (Boutilier 2011; Diwan & Ramesh 2009).

3.1.2. *Effect of freestream turbulence intensity*

In the presence of freestream turbulence forcing the mean flow toplogy of the LSB changes, in particular a slight delay of boundary layer separation is observed, the height of the LSB decreases significantly and the mean transition position advances upstream as can be observed in the contours of mean streamwise velocity and the u_{rms} are presented in Fig. 7. For the sake of brevity only three configurations are presented, C1 (Tu = 1.21%), C5 (Tu = 2.97%), and C7 (Tu = 6.26%) where no laminar separation bubble is observed. The measurements, in accordance with previous studies (Istvan & Yarusevych 2018; Simoni *et al.* 2017; Hosseinverdi & Fasel 2019), show that with the increase of Tu, the streamwise extent of the separation bubble is reduced, and a result of an earlier onset of pressure recovery, caused by the shear layer transitioning in the aft position of the LSB. The length of the bubble will decrease due to higher initial forcing or higher amplification rate. This will have an impact on the reattachment point, leading to shorter bubble. The displacement effect of the boundary layer will be reduced and will modify the pressure gradient and the re-adjustment will result in the small change in the location of the separation. This has been reported quite widely in the literature but Marxen & Henningson (2011) have shown quantitative validation where they studied the effect of varying the magnitude of initial perturbation. This phenomena will be investigated in more detail in the next section. Finally, the height of the LSB is also reduced, and has been also observed in previous experimental and numerical studies (Istvan & Yarusevych 2018; Simoni *et al.* 2017; Hosseinverdi & Fasel 2019).

Recent experimental studies by Simoni *et al.* (2017) show that the change of mean separation position with an increase of Tu was too small to be measured, where Istvan & Yarusevych (2018) found that an increase in Tu results in a slight shift downstream of the separation which is closer to what has been observed in previous studies (Hosseinverdi & Fasel 2019), albeit with a large experimental uncertainty. Any small delay in boundary layer separation is thought to be due to the increased initial energy amplitude introduced into the boundary layer due to the FST, resulting in separation to occur further downstream, shortening the bubble due to the earlier transition. The resulting boundary layer displacement effect modifies the upstream pressure field leading to separation delay. Current measurements approximate that separation location is shifted from $0.375c$ to $0.425c$, with the exact location not being possible due to the uncertainty of the measurements. However as mentioned in the previous section, the location of the separation position would have little impact on the boundary layer transition mechanisms, hence it is not of great interest in the present study.The reattachment point is somewhat easier to determine as its variation with Tu is larger than for the separation point as the inflectional nature of the profile is not clearly distinguishable. In the current configuration the reattachment point for the configurations where an LSB was observed are presented in Table 3. Referring to the boundary layer integral parameters presented in Fig. 8, the streamwise location of the peak in the displacement thickness (δ_1) is accompanied by an increase in momentum thickness (δ_2), and can be associated to the mean transition of the separating shear layer. Consequently the shape factor ($H = \delta_1/\delta_2$) also reaches a maximum value at this position, corresponding to the maximum height of the laminar separation bubble. Increasing the level of Tu results in a systematic decrease in δ_1, corresponding to the decrease in the wall-normal height of the LSB. Additionally, a higher Tu results in a less pronounced value of δ_1 and an upstream shift in the location of the maxima. This combined, with an earlier onset of momentum thickness growth, indicates earlier transition. When the levels of Tu passed a certain threshold, existence of a laminar separation bubble is in question as H does not exhibit any streamwise growth. In the current experimental configuration the level of Tu at which the bubble was suppressed is 4.26% (C6). Configuration C5 (Tu = 2.97%) could still have an LSB as an amplified frequency band

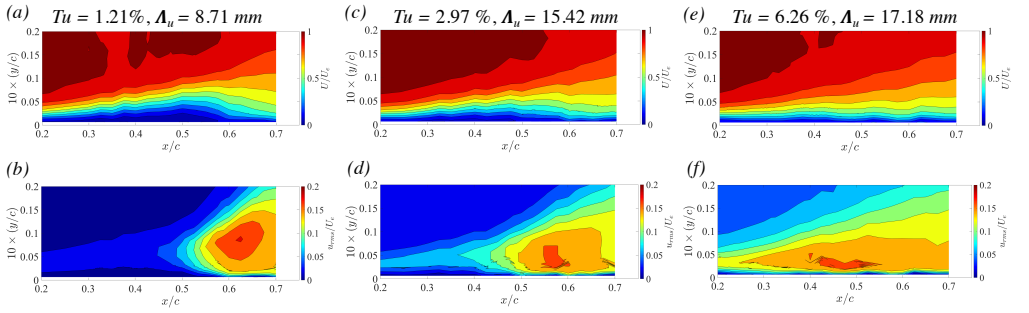

Figure 7: Contours of the mean streamwise velocity (U) and the r.m.s of the fluctuating streamwise velocity (u_{rms}) for exemplary configurations subjected to elevated levels of FST (a) 1.21% (b) 2.97% and (c) 6.28%

$Tu(\%)$	x_S/c	x_T/c	x_R/c
0.15	0.375	0.575	0.700
0.64	0.375	0.525	-
1.21	0.400	0.475	0.600
1.23	0.400	0.475	0.600
1.31	0.400	0.475	0.600
1.63	0.400	0.475	0.575
2.97	0.425	0.425	0.500

Table 3: Effect of freestream turblence on mean streamwise locations of separation ($x_S \pm 0.07$), mean transition ($x_T/\pm 0.025$) and reattachment ($x_R/c \pm 0.025$). NB. The reattachment position was not measured in the configuration with $Tu = 0.64\%$.

is observed in the power spectral density and will be discussed in more detail in Section 3.2. Furthermore, for all the configurations, H departs from a value expected for a laminar boundary layer ($H > 2.5$) and asymptotically levels of those expected of a turbulent boundary layer ($H < 2$), signifying that transition occurs within the HWA measurement domain. The current results exhibit the same systematic trends in mean bubble topology and integral parameters as in the DNS of Hosseinverdi & Fasel (2019) and PIV measurements of Istvan & Yarusevych (2018).

Upon inspection of the u_{rms} profiles in the wall-normal direction from Fig. 9, increasing the Tu results in an upward shift in the maxima. This behaviour suggests a shift in the transition mechanism, where a non-modal instability would exhibit the maximum u_{rms} values further away from the wall than a viscous modal instability. Moreover, increasing the freestream turbulence intensity yields magnitudes of $u_{rms}/U_e \approx 10\%$ which is common for streaks (Westin *et al.* 1993; Fransson *et al.* 2005), and is larger than what is observed for pure modal transition ($u_{rms}/U_e \approx 1\%$, Arnal & Julien (1978)). The co-existence of modal and non-modal instabilities in attached boundary layers have been found to have similar effects on the maxima of the u_{rms} peak (Veerasamy *et al.* 2021). In the configurations where the Tu is large enough to suppress the bubble, the u_{rms} peak gradually shifts downwards, suggesting the flow is undergoing transition through an inviscid (Kelvin-Helmholtz) or viscous (Tollmien-Schlichting) instability and will be discussed later. Finally, increasing the Tu decreases the rate at which the fluctuations diminish into the freestream.

Using acoustic forcing, Kurelek *et al.* (2018) found that the initially increased amplitude in the boundary layer upstream of the flow resulted in the bubble being shorter and thinner,

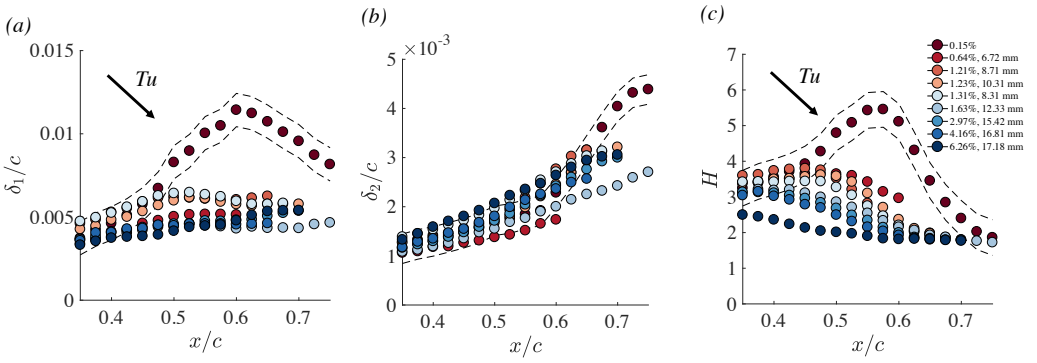

Figure 8: Effect of freestream turbulence on integral shear layer parameters: (a) displacement thickness (δ_1), (b) momentum thickness (δ_2) and (c) shape factor (H). Turbulence intensity increases from dark red to dark blue, refer to Table. 2. Dashed lines denote uncertainty for the natural case.

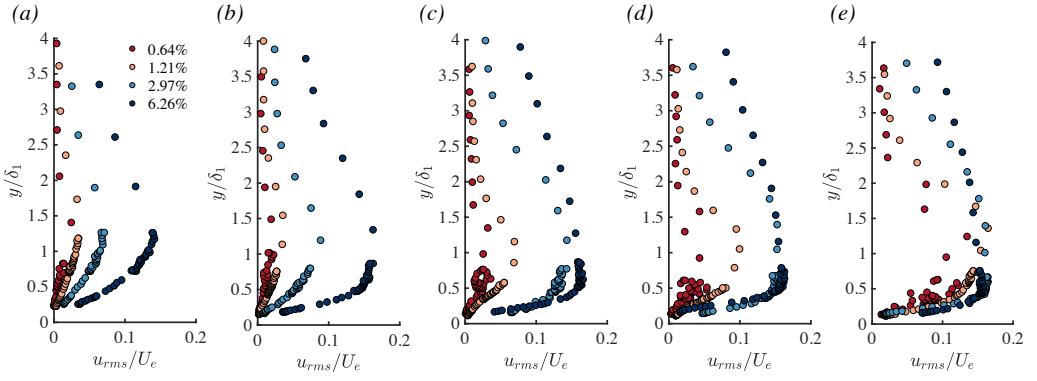

Figure 9: Chordwise development of the r.m.s of the fluctuating streamwise velocity component (u_{rms}) for chordwise positions of (a) 0.250c (b) 0.350c (c) 0.425c (d) 0.500c and (e) 0.575c subjected to freestream turbulence.

similar to what has been observed in Marxen & Henningson (2011) in DNS simulations. In the same manner, freestream turbulence increases the initial forcing in the boundary layer resulting in similar effects on the mean flow topology as with different forcing techniques. The impact of forcing on the wall-normal height of the bubble would modify the type of modal instability mechanism since in a separated boundary-layer profile, the eigenfunctions can recover features of both Tollmien-Schlichting and Kelvin-Helmholtz instabilities where height of the bubble is related to which amplifying mechanism dominates the transition process (Rist & Maucher 2002).

3.2. *Disturbance growth and instability*

3.2.1. *Spectral analysis*

The power spectral density (PSD) of the streamwise velocity fluctuations was calculated for each configuration, with the chordwise evolution presented in Fig. 10. In the cases where an LSB was present, the PSD exhibits a characteristic frequency band amplified downstream (cf. Fig. 10a-g). When the LSB was subjected to FST, the chordwise development and distribution of the spectra were significantly modified. First, the unstable frequency band is broadened, which is a consequence of significant energy content within a broader range of frequencies in

the FST, resulting in measurable velocity fluctuations over a broader frequency range earlier upstream. Second, increasing the freestream turbulence level results in the unstable frequency band being slightly shifted to a higher frequency range than the natural case. For example, increasing the freestream turbulence level from the baseline to a value of $Tu = 1.23\%$ results in the frequency band being shifted from $110 - 150Hz$ to $160 - 200Hz$ (cf. Fig. 10a and d). Referring to Fig. 10a-g, the unstable frequency band is propagated upstream of the separation point due to the separation bubble's streamwise oscillation. The highest frequency wave packet is found to occur in the highest Tu case, which was $255 - 295Hz$, wherein the highest cases ($Tu > 4\%$, Fig. 10h, i) no clear frequency band is observed and is thought to be due the LSB not being present anymore, inferring a change in the instability mechanism. The frequency shift of the wave packet is attributed to the decreased size of the LSB and has been observed in Hosseinverdi & Fasel (2019). Current results suggest that in the configurations that are subjected to a turbulence intensity of $Tu < 3\%$, the harmonic of the frequency band is still observed (cf. Fig. 10 b,f and e), which could suggest that in the presence of moderate levels of FST the secondary instability of the primary modal instability could still be present. The secondary instability, a harmonic of the leading frequency, takes effect in the aft portion of the bubble where vortex shedding occurs. It has been reported to be an elliptic instability (Marxen & Henningson 2011), amplifying disturbances with spanwise wavelengths on the order of the diameter of the shed vortices, resulting in spanwise distortion and waviness in the vortex filament. The presence of streaks would result in spanwise inhomogeneity, inhibiting elliptic instability. The current results indicate that if the Tu is increased to a certain level, the harmonic of the wave packet is barely noticeable (cf. Fig.10g), suggesting that there is a certain threshold of FST forcing which will "bypass" the elliptic instability, which will still exist in moderate cases and is in agreement the numerical simulations of Li & Yang (2019). Additionally, as in Balzer & Fasel (2016), possible harmonics are observed in the spectra for the LSB subjected to FST. The impact of the integral length scale has a negligible effect on the unstable frequency range of the wave packet.

Pauley *et al.* (1990) proposed a scaling of the most unstable frequency in an LSB, in the form of a Strouhal number defined as:

$$St_{\delta_2,sep} = \frac{F\delta_{2,sep}}{U_{e,sep}} \tag{3.1}$$

where F is the most amplified frequency observed in the experiment, $\delta_{2,s}$ and $U_{e,s}$ are the momentum thickness and boundary layer edge velocity at separation, respectively. Inspired by the analysis of Rodríguez & Gennaro (2019) and Rodríguez *et al.* (2021), who compared the value of the St_{δ_2} for past experiments on LSBs, Fig. 11 compares the value of St_{δ_2} as a function of Tu (for the cases where an LSB was observed). In the present work, $St_{\delta_2} = 0.0062$, for the unforced bubble, which is close to the value of $St_{\delta_2} = 0.0069$ proposed by Pauley *et al.* (1990) for 2D numerical simulations of a laminar separation bubble. However, increasing the Tu causes St_{δ_2} to increase, when compared to the baseline case, approaching values closer to what was proposed by Rodríguez *et al.* (2021) of $St_{\delta_2} = 0.01 - 0.012$ for a bubble acting as a global oscillator. Data from Istvan & Yarusevych (2018) also suggest this effect and Pauley (1994) found that $St_{\delta_2} = 0.0124 - 0.0136$ in 3D unforced numerical simulations twice as large of what was observed for 2D simulations. Therefore, the increased values of St_{δ_2} suggest that the presence of freestream turbulence (or increased levels of forcing) could favour the inherent three-dimensional nature of the transition process in the LSB. Furthermore, Rodríguez & Gennaro (2019) found that increasing the recirculating velocity in the bubble increased the values of St_{δ_2} which could manifest here as well as the LSBs subjected to FST are smaller in size for the same convective velocity, which could result

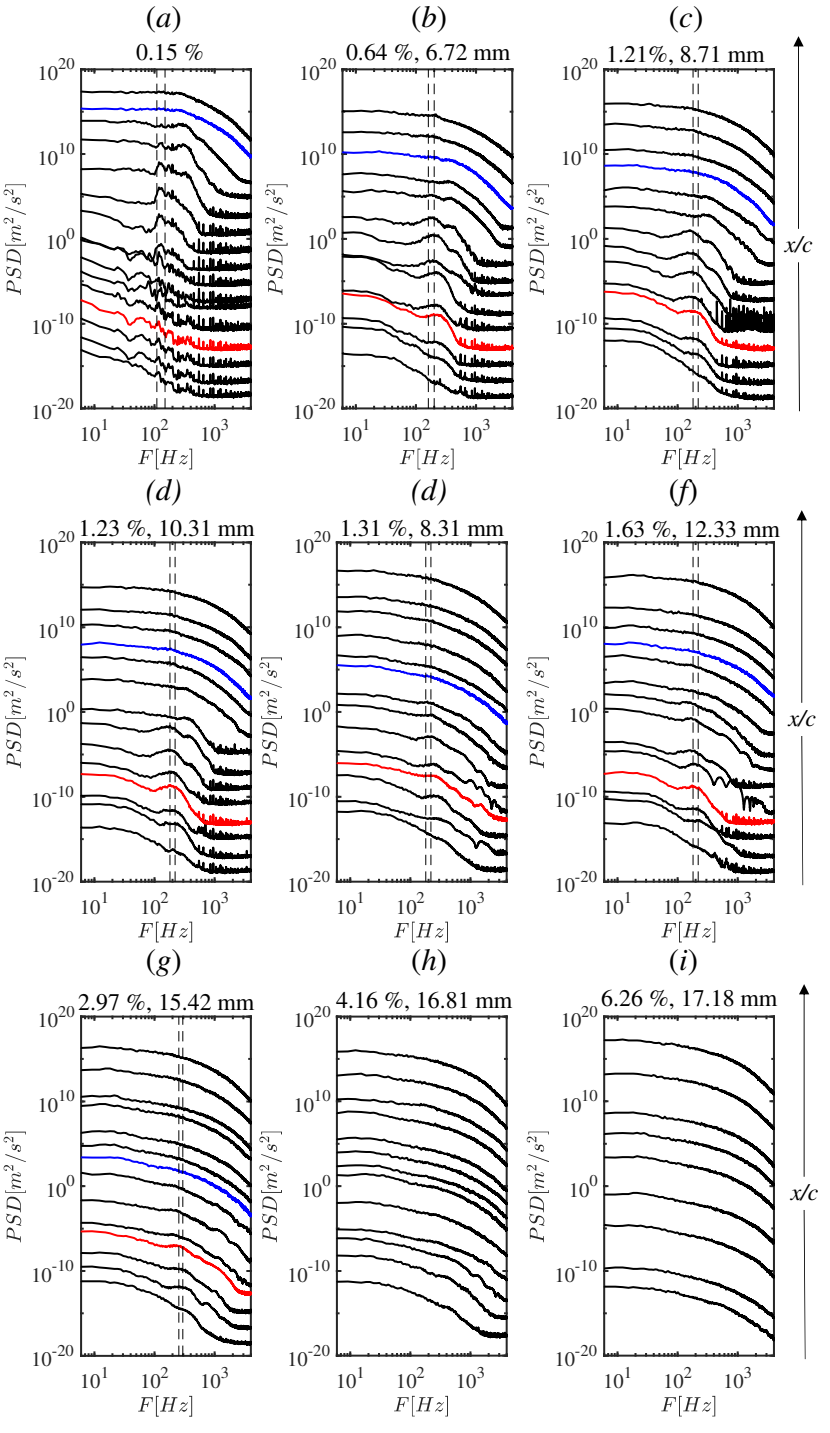

Figure 10: Chordwise evolution of the Power Spectral Density (PSD) at the maximum location of u_{max} inside the boundary layer for each configuration. Where the frequency bands correspond to the vertical dashed lines which indicate the most amplified frequency band used in the stability analysis in the following section. Red and blue curves denote x_S and x_R, respectively. NB: Spectra are separated by an order of magnitude for clarity.

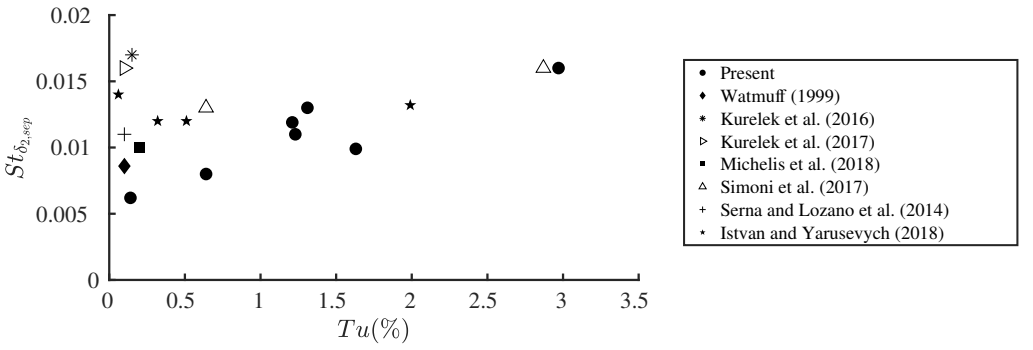

Figure 11: The dimensionless frequency, St_{δ_2}, plotted against the turbulence intensity, Tu, for the present results and experimental data from the literature.

in larger levels of re-circulation inside the bubble. Finally, discrepancies in the values of St_{δ_2} can be associated with the fact that the different experiments in the literature were conducted on flat plates (with imposed pressure gradients) and aerofoils, the surface finish of the models, and the inherent bias of the different experimental techniques. Moreover, the different Reynolds numbers and pressure gradients would modify the mean bubble's height and length, which could also result in the differences in the value of St_{δ_2}. In particular, under certain conditions (Gaster 1967), the formation of a "long" bubble can occur. However, it is out of the scope of the current study, which focuses on a "short" bubble.

The global displacement of the separated shear layer in an LSB is often referred to as flapping and is known to occur at significantly lower frequencies than the 2D vortex roll-up and shedding (Zaman *et al.* 1989; Michelis *et al.* 2017). The frequency of the flapping of the bubble can be expressed using a Strouhal number based on the displacement thickness:

$$St_{\delta_1,sep} = \frac{F\delta_{1,sep}}{U_{e,sep}} \tag{3.2}$$

which follows the conventions used in Michelis *et al.* (2017) and should not be confounded with the Strouhal number proposed by Pauley *et al.* (1990). Moreover, for assessing flapping experimentally, a temporal signal is extracted at a streamwise location corresponding to the approximate position of the mean separation point, x_s, and at a wall-normal location of $y = \delta_1$. At this same position in the LSB, Michelis *et al.* (2017) demonstrated that the flapping of an unforced LSB manifested itself at low frequencies or $St_{\delta_{1,s}} \approx 0.005$. The results shown in Fig 12 suggest that flapping is also manifesting at similar values as a distinct peak is present at $St_{\delta_{1,s}} \approx 0.006$. Moreover, the addition of freestream turbulence significantly modifies the signal's spectral content, with no distinct peaks being present, suggesting that FST could modify bubble flapping, resulting in damping or reducing the global displacement of the separated shear layer.

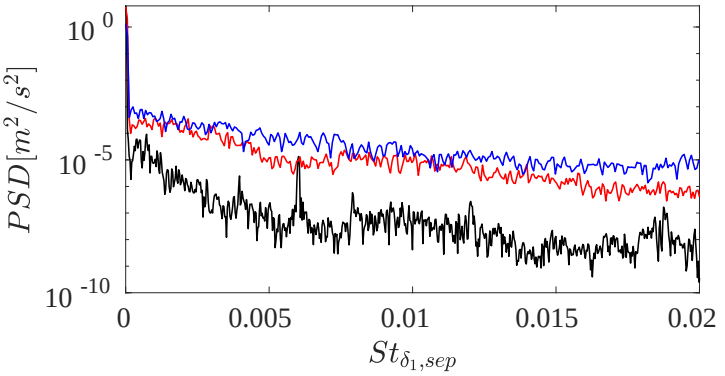

Figure 12: Power spectral for the unforced LSB (black), the LSB subjected to $Tu = 0.64\%$ (red) and $Tu = 1.21\%$ (blue) at a height of $y = \delta_1$ at the separation point. NB: The Strouhal number is scaled by δ_1, and should not be confounded with the Strouhal number scaled with δ_2 in Fig. 11

3.2.2. *Disturbance energy growth*

The effect of increasing the level of Tu on the chordwise evolution of the disturbance energy growth ($E = u^2_{rms}/U^2_e$) is presented in Fig. 13a, where the trend of disturbance growth gradually changes from exponential, at lower levels of Tu, to algebraic for the more extreme Tu levels, where energy saturation is observed earlier. These different energy growth behaviours suggest that different instability mechanisms were present in the flow, and their contribution to the transition process depends on the level of the freestream forcing. Figure 13b shows the energy growth of the filtered disturbances for the most amplified frequency band (corresponding to the modal instability in the LSB) obtained from the PSD (cf. Fig.10). In the natural case, low levels of disturbance growth are present before the separation point, and further downstream, exponential amplification of the disturbances is observed. In the cases where the flow is subjected to additional FST, the initial energy amplitude is significantly higher than in the natural case. The initial energy in the boundary layer increases with Tu, with higher energy levels suggesting the presence of streaks, as commonly observed in experiments on transition induced by FST in boundary layers subjected to no adverse pressure gradient.

Referring to Fig. 13b, the gradual reduction in the slope of the chordwise energy growth with increasing Tu would suggest that the non-modal instabilities become more dominant, which can be thought of as being in competition with the modal instabilities which grow exponentially. Once the turbulence forcing reaches a critical level, the exciting streaks in the boundary layer are too energetic to allow the flow to separate, resulting in the elimination of the modal via the non-modal instability (in the present work, approximately when $Tu > 4\%$, as no inflexion point is observed in the bubble is observed in the mean flow and no amplified frequency band in the PSD). Damping of the modal disturbance growth is attributed to the mean flow deformation due to the influence of freestream turbulence. In other words, external freestream turbulence forcing reduces the size of the separation bubble, such that the region of instability growth is brought closer to the wall, resulting in damping effects of the disturbances in the shear layer. Previous experiments on forced bubbles found a damping effect on the disturbance growth. For example, Kurelek *et al.* (2018) found that both tonal and broadband acoustic forcing resulted in the damping of modal disturbances along with Yarusevych & Kotsonis (2017) and Marxen & Henningson (2011) who used a variety of forcing techniques to observe similar behaviour. Furthermore, the DNS investigation by Hosseinverdi & Fasel (2019) found similar trends in the energy growth with increased levels

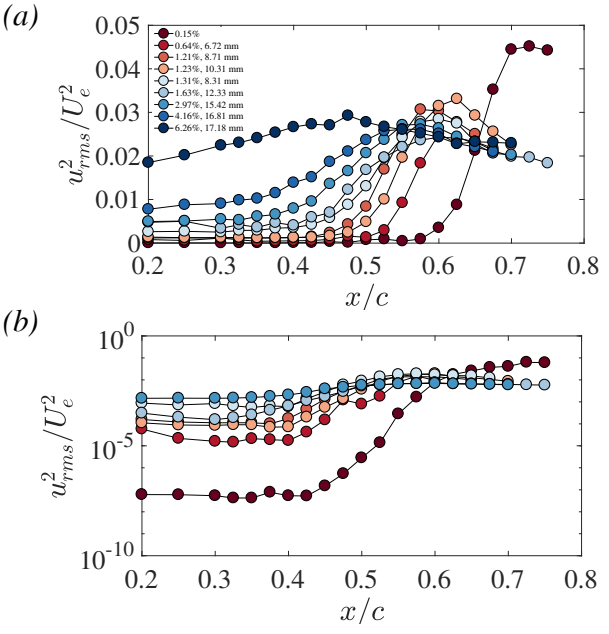

Figure 13: Energy growth of disturbances for a) integrated over the entire energy spectrum and b) integrated over the frequency range of the most amplified wave packet plotted on a semi-log scale to show modal growth. NB: configurations where no LSB was detected ie. where no amplified frequency band was observed in the PSD are not included for the filtered disturbance growth (cf. Fig. 10h,i). Maximum values of u_{rms} in the boundary layer are presented.

of *Tu*, albeit they did not show the behaviour when the bubble was suppressed, which in the present results is characterised by a high level of initial energy and evident algebraic growth of disturbances upstream of any possible separation location ($Tu = 6.26\%$, Fig. 13a).

The damping of the modal disturbances in the bubble could be due to the presence of streaks (Klebanoff modes) caused by the elevated levels of freestream turbulence, which would introduce non-modal disturbances into the boundary layer. In the current setup, streaks should appear for configurations where $Tu > 1\%$ is a common threshold for zero-pressure gradient boundary layers (Matsubara & Alfredsson 2001; Fransson *et al.* 2005). The behaviour of the disturbance growth suggests the co-existence of modal and non-modal instability in the LSB when subjected to a critical level of freestream turbulence. The experimental findings here agree with previous numerical results in the literature (Hosseinverdi & Fasel 2019; Li & Yang 2019; Balzer & Fasel 2016).

The impact of the integral length scale for a relatively constant *Tu* level on the disturbance growth is presented in Fig. 14, suggesting that the effect of the integral length scale on the transition in an LSB is very modest. The difficulty in achieving constant levels of *Tu* with a varying Λ_u is an experimental challenge, as shown by Fransson & Shahinfar (2020). The present work investigates three cases with a minimal variation in *Tu* and a larger variation in Λ_u. It is observed that an increase in Λ_u at the leading edge of the aerofoil for an almost constant *Tu* appears to delay the growth and eventual saturation and breakdown of the disturbances and is in agreement Breuer (2018), who suggested that the smaller scales were closer to that of the shear layer resulting in the receptivity of the boundary layer to increase. The impact of Λ_u has been shown to have contradicting results in attached boundary layer transition problems, where a variation of the integral length scale both advances (Jonáš

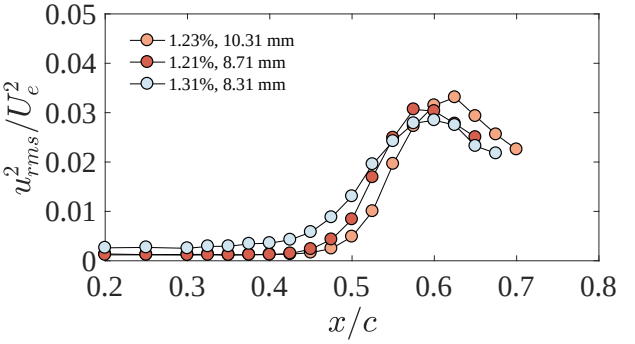

Figure 14: The chordwise evolution of the disturbance energy growth for configurations with a relatively fixed *Tu* and varying Λ_u. NB: Maximum values of u_{rms} in the boundary layer are presented.

et al. 2000; Brandt *et al.* 2004; Ovchinnikov *et al.* 2008) and delays (Hislop 1940; Fransson & Shahinfar 2020) boundary layer transition. This contradiction led Fransson & Shahinfar (2020) to hypothesise a two-fold effect of the integral length scale on boundary layer transition subjected to freestream turbulence. They found that for a constant *Tu* level, an optimal scale ratio exists between the Λ_u at the leading edge and the boundary layer thickness δ at the transition position, which has a value of approximately 12.5. Interestingly, in the attached portion of the boundary layer of the three configurations tested, the advancement of the non-linear growth of disturbances and eventual breakdown occurs when approaching this optimal value.

However, it should be noted that the above studies were conducted on attached boundary layers. Hence it is unclear whether meaningful comparisons can be made. For laminar separation bubbles, Hosseinverdi & Fasel (2019) briefly suggested that the integral length scales ranging from $0.9\delta_1$ to $3\delta_1$ had little effect on the energy growth relative to the *Tu*, and is also observed in the experimental results here. Furthermore, a smaller integral length scale resulted in a higher initial level of disturbance energy in the boundary layer and has also been observed by Hosseinverdi (2014), however in their work, the saturation of the energy growth was found to be independent of Λ_u. Based on the experimental observations here and past numerical simulations, an effect of the integral length scale could be present, and further investigation is warranted. However, it is likely that the effect will be small compared to the *Tu*, in light of the results here and Hosseinverdi & Fasel (2019).

3.2.3. *Co-existence of a modal and a non-modal instability*

The assertions made in the previous sections on the co-existence of modal and non-modal growth of disturbances in the laminar separation bubble will be examined here through a linear stability analysis. Linear Stability Theory (LST) models the amplification of small amplitude disturbances (Schmid & Henningson 2000) and has been employed to study the convective streamwise amplification of disturbances in the LSB. The Orr-Sommerfeld given by Eq. 3.3 can reliably predict the primary amplification of instability waves for parallel flows and in the fore position of an LSB (Kurelek *et al.* 2018).

$$\left(U-\frac{\Omega}{\alpha}\right)\left(\frac{d^2\tilde{v}}{dy^2}-\alpha^2\tilde{v}\right)-\frac{d^2U}{dy^2}\tilde{v}=-\frac{iU_e\delta_1}{\alpha Re_{\delta_1}}\left(\frac{d^4\tilde{v}}{dy^4}-2\alpha^2\frac{d^2\tilde{v}}{dy^2}+\alpha^4\tilde{v}\right) \tag{3.3}$$

where Re_{δ_1} is the Reynolds number based on displacement thickness, $\tilde{v}$ is the wall-normal perturbation, Ω is the angular frequency, and the complex wave number is defined as $\alpha = \alpha_r + i\alpha_i$, where i is the imaginary unit. When $\alpha_i > 0$, the disturbance is attenuated and amplified when $\alpha_i < 0$.

Calculations were conducted using ONERA's in-house stability code, where a spatial formulation of the problem is employed (Schmid & Henningson 2000), such that Ω is defined and the eigenvalue problem is solved for α, therefore modelling the convective amplification of single frequency disturbances. Equation 3.3 is solved numerically using Chebyshev polynomial base functions and the companion matrix technique to treat eigenvalue non-linearity (Bridges & Morris 1984).

The mean streamwise velocity profiles at discrete streamwise locations are used as input for the LST calculations, making the analysis local, with the same methodology employed by Yarusevych & Kotsonis (2017) and Kurelek *et al.* (2018). Stability calculations are highly sensitive to noise due to the spatial resolution in experiments. Therefore the LST analysis is conducted using hyperbolic tangent fits on experimental data, which have shown to provide reasonable stability predictions, being relatively insensitive to scatter in experimental data. The following modified hyperbolic tangent fit was used:

$$\frac{U}{U_e}=\frac{tanh[a_1(y-a_2)]+tanh[a_1a_2]}{1+tanh[a_1a_2]}+a_3\frac{y}{a_2}exp[-1.5\frac{y}{a_2}^2+0.5] \tag{3.4}$$

which was proposed by Dovgal *et al.* (1994) and has been shown to suitably model separated boundary layer profiles in several analytical applications Boutilier (2011); Boutilier & Yarusevych (2013) along with accurate linear stability predictions on HWA velocity profiles of separated shear layers (Boutilier & Yarusevych 2012; Methel *et al.* 2019). The profile edge velocity, U_e, is estimated from the HWA measurements, while the coefficients $a_1 - a_4$ are estimated through a least-squares curve fitting operation to the measured data. Exemplary velocity profiles and their corresponding fits for the configuration with Tu=1.23% are presented in Fig. 15. Furthermore, due to the difficulty in conducting stability calculations on experimental velocity profiles at low Tu and Reynolds numbers, LST calculations for the baseline case are validated by conducting the analysis on both experimental and numerical (obtained from the boundary-layer solver, 3C3D) velocity profiles which demonstrate agreement between the amplification rate and the most amplified frequencies.

A measure of the amplitude growth is quantified from LST through the computation of amplification factors and will be referred to as the $N-$factor hereinafter. The $N-$factor as a function of streamwise position (x) and frequency (F) from LST calculations and is quantified

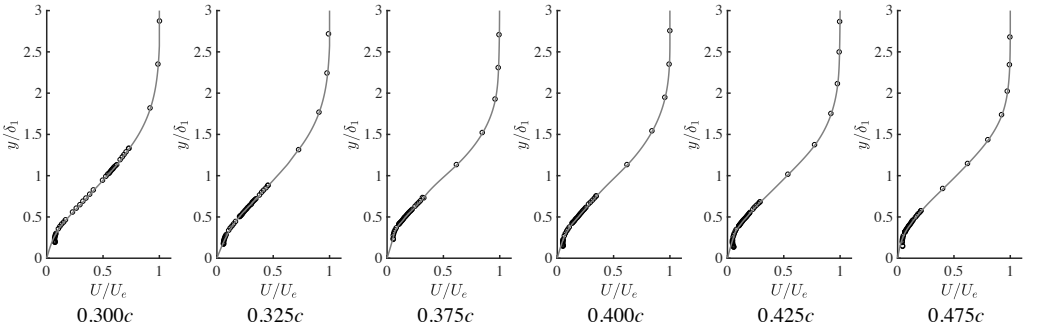

Figure 15: Measured mean velocity profiles (markers) in a forced condition ($Tu = 1.21\%$) and corresponding hyperbolic tangent fits (solid lines) used in LST computations.

by integrating α_i for the most amplified frequency in the positive $x-$direction:

$$N(x, F) = \int_{x_{cr}}^{x} -\alpha_i \, dx \tag{3.5}$$

where x_{cr} is the critical abscissa and corresponds to the location at which a perturbation at a frequency of Ω is first amplified. The location of x_{cr} is upstream of the hot wire measurement region and, therefore, cannot be determined directly. However, as demonstrated by Jones *et al.* (2010), Kurelek *et al.* (2018), Yarusevych & Kotsonis (2017) and Kurelek (2021), in the fore portion of the LSB the streamwise evolution of α_i can be approximated by a second order polynomial. For example, Kurelek (2021) (HWA, Ch. 6) and Kurelek *et al.* (2018) (PIV) demonstrated that the $(-\alpha_i)$ obtained from LST calculations for four velocity profiles before and after the separation position could be used in the interpolation. Considering this, x_{cr} can be determined by extrapolating the fit to $\alpha_i = 0$. Experimentally, the $N-$factor is calculated as $N(x) = ln(A(x)/A_{cr})$, where $A(x)$ denotes the maximum disturbance amplitude in the boundary layer for a given frequency band (band-pass filtered u_{rms}) and A_{cr} denotes the initial disturbance amplitude that becomes unstable. A direct comparison of $N-$factor obtained from LST and experiment is not possible since, experimentally, the initial disturbance amplitude is not known and likely to be too small to be measured, only being detected well downstream of x_{cr}. Nevertheless, following Schmid & Henningson (2000), $N-$factors are matched at a reference location where the disturbance amplitude reaches $0.005U_\infty$, consequently allowing for an estimate of A_{cr} for a given frequency band. Finally, only $N-$factors based on the streamwise component are possible since the hot wire does not measure a vertical component.

In the baseline configuration (cf. Fig. 16a, NB. the figures show both the energy in the spectra and the N-factor and direct comparisons between their magnitudes are not to be made; only the frequencies at which the largest magnitudes occur), the overlaid plot between PSD and the N-factor show that LST is capable of predicting the most amplified frequencies from experiment, with acceptable accuracy (10% difference). For example, Kurelek *et al.* (2018) and Yarusevych & Kotsonis (2017) found a difference of 17%, while stating this to be an acceptable range. A comparison with experimental $N-$factors further supports the validity of the LST predictions (cf. Fig. 17a), which reveals that the linear growth of disturbances is captured between $0.475 < x/c < 0.525$, comparable to the same analysis by Kurelek *et al.* (2018) who found LST to accurately capture the growth of disturbances between $0.42 < x/c < 0.46$ in the experiment. Furthermore, the downstream saturation of the experimental $N-$factors begins to deteriorate the agreement between LST due to non-linear effects becoming significant. The eigenfunction of the most amplified frequency

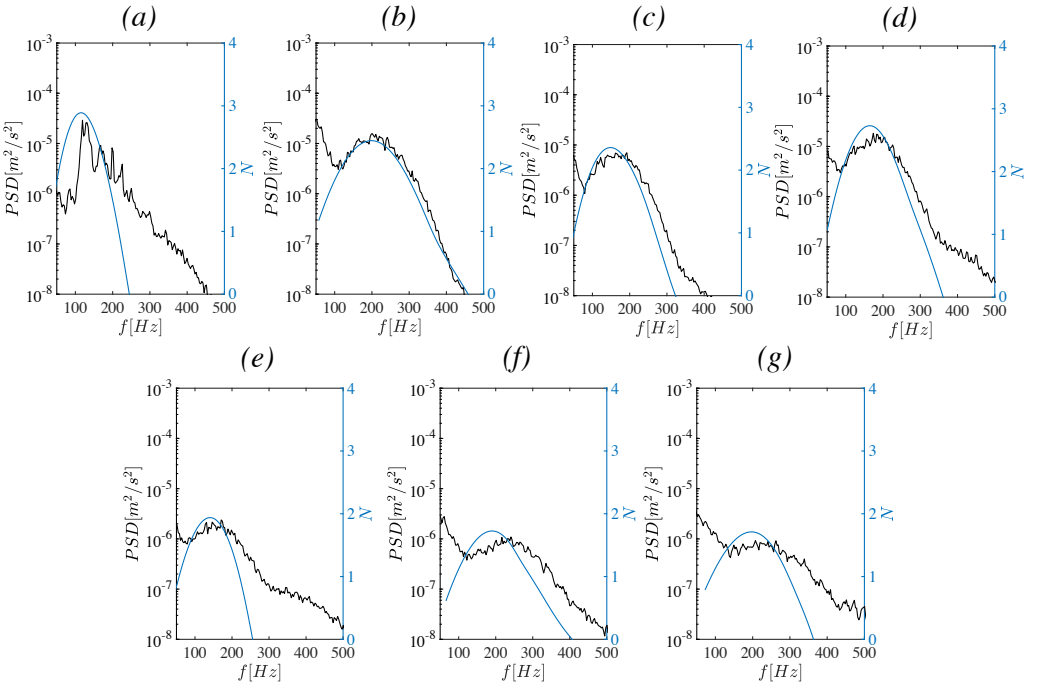

Figure 16: Comparison between the amplified frequencies predicted by LST to the experimental spectra for (a) Natural case ($x = 0.400c$) ; (b) $Tu = 0.64\%\Lambda_u = 4.6mm$ ($x = 0.425c$) ; (c) $Tu = 1.21\%\Lambda_u = 8.7mm$ ($x = 0.425c$); (d) $Tu = 1.23\%$, $\Lambda_u = 10.3mm$ ($x = 0.425c$); (f) $Tu = 1.63\%$, $\Lambda_u = 12.3mm$ ($x = 0.425c$); (g) $Tu = 2.97\%$, $\Lambda_u = 15.4mm$ ($x = 0.400c$). NB: Two different $y-$axes for α_i and the power from the PSD, therefore direct comparisons between the two are not be made.

predicted by LST is presented in Fig 18a, and is in acceptable agreement with the experiment for filtered fluctuating streamwise velocity profile in the wall-normal direction for the most amplified frequency band. The eigenfunction exhibits two distinct peaks at approximately $y/\delta_1 = 1$, corresponding roughly to the inflection point and $y/\delta_1 = 0.3$, which is indicative of a viscous modal instability (Veerasamy *et al.* 2021). Rist & Maucher (2002) showed that LSBs with smaller wall normal distances could exhibit Tollmien-Schlichting waves instead of an inviscid Kelvin-Helmholtz instability for higher wall normal distances. Therefore, based on the agreement seen in disturbance unstable frequencies, eigenfunctions and amplification rates (Figs. 16a, 18 and 17a), it is established that the employed LST analysis is justified for determining stability characteristics in the fore portion of the LSB.

For the configurations where the LSB is subjected to elevated levels of freestream turbulence, LST can predict the most amplified frequencies, spatial amplification and eigenfunctions, suggesting that a modal instability is still present at elevated levels of freestream turbulence when the bubble is present. Counter-intuitively, freestream turbulence forcing results in better agreement between LST and experiment and has been found in past experiments with increased forcing by Yarusevych & Kotsonis (2017); Kurelek *et al.* (2018) and Kurelek (2021) (Ch. 6), who found that LST was capable of predicting the convective growth of disturbances in LSBs subjected to plasma, tonal and broadband acoustic forcing. However, as Kurelek *et al.* (2018) noted, the critical caveat to be considered is that the degree to which LST and experiment agree is entirely dictated by the relevance of non-linear effects for the particular disturbance mode being considered. Fully developed freestream

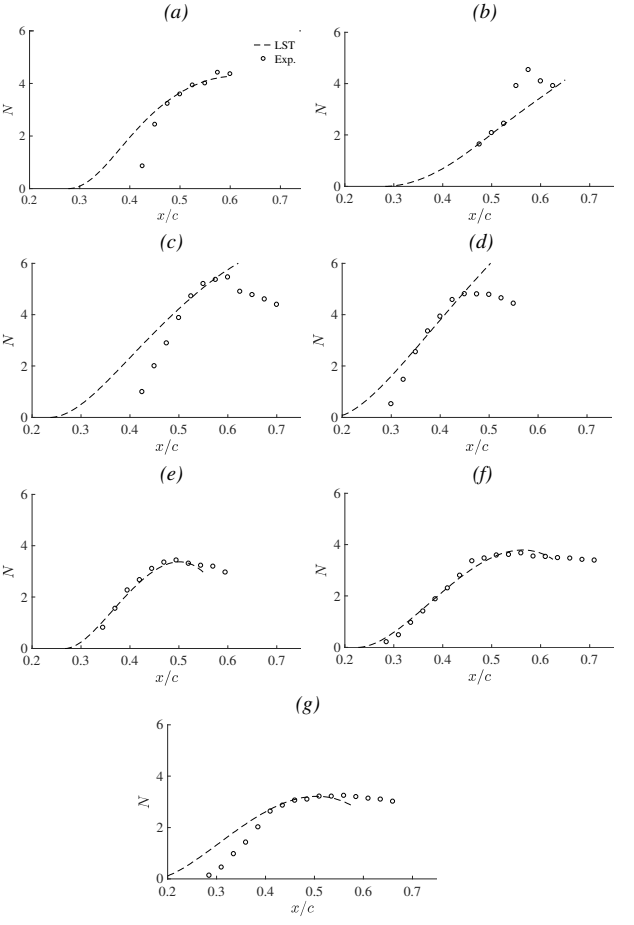

Figure 17: Comparison of experimental (markers) LST (dashed line) predicted $N-$factors for frequencies within the excitation bands from Fig. 10 for configurations where a laminar separation bubble is present (a) Natural case; (b) $Tu = 0.64\%\Lambda_u = 4.6mm$; (c) $Tu = 1.21\%\Lambda_u = 8.7mm$; (d) $Tu = 1.23\%, \Lambda_u = 10.3mm$; (e) $Tu = 1.31\%, \Lambda_u = 8.3mm$; (f) $Tu = 1.63\%, \Lambda_u = 12.3mm$; (g) $Tu = 2.97\%, \Lambda_u = 15.4mm$; Initial disturbance amplitudes are estimated through matching LST and experimental $N-$factors

turbulence could act as a type of "broadband" forcing, such that all unstable disturbance amplitudes are small, resulting in non-linear effects and an improved agreement between LST and experiment. Therefore, current results support the assertions made by Kurelek *et al.* (2018), who found excellent agreement between LST and experiment for an LSB subjected to broadband acoustic forcing. The higher signal-to-noise ratio can also explain the improvement in the presence of forcing with freestream turbulence.

Another, perhaps more probable, explanation for the divergence between LST and experiment for configurations subjected to low levels of Tu could result from the bubble's wall-normal extent being more considerable compared to higher levels of Tu. The more considerable distance of the shear layer from the wall would foster other instabilities, such as a global oscillator (Rist & Maucher 2002) or a three-dimensional global instability preceded by a global oscillator (Rodríguez *et al.* 2021). Another possibility could be that a shear on structures in the direction opposed to the mean flow may lead, through an Orr mechanism (Cherubini *et al.* 2010), to a non-modal instability. Therefore, the augmented agreement

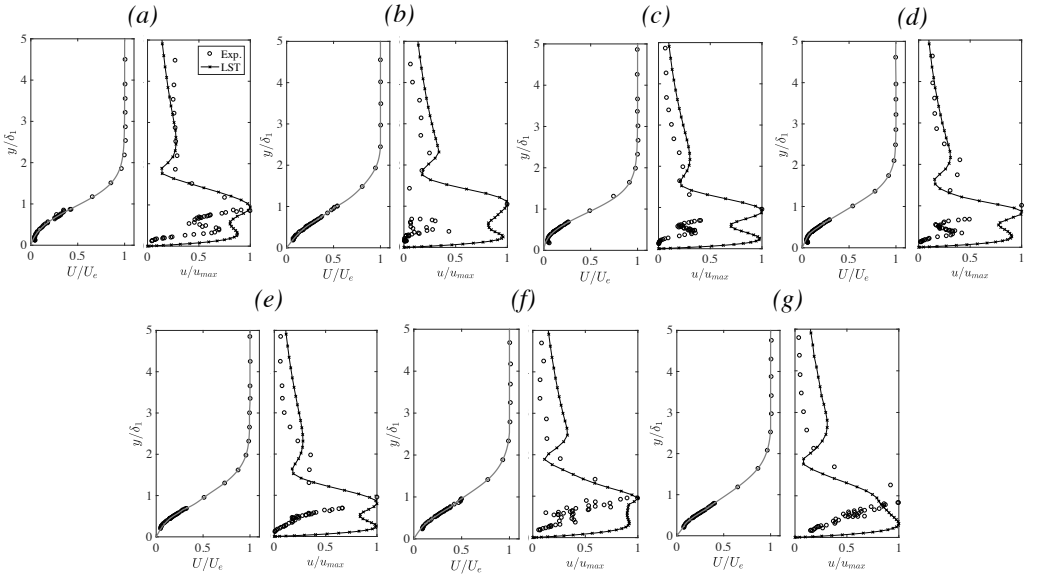

Figure 18: Experimental filtered disturbance profiles in the wall-normal direction compared to the eigenfunction for the most amplified frequency from LST. Experimental streamwise disturbance profiles are computed by applying a bandpass filter corresponding to the lost amplified frequency band from the PSD. (a) Natural case; [110 - 150 Hz]; (b) Tu = 0.64%, Λ_u = 4.6mm [160 - 200 Hz]; (c) Tu = 1.21%, Λ_u = 8.7mm [180 - 220 Hz]; (d) Tu = 1.23%, Λ_u = 10.3mm [180 - 220 Hz]; (e) Tu = 1.31%, Λ_u = 8.3mm [180 - 220 Hz]; (f) Tu = 1.63%, Λ_u = 12.3mm [180 - 220 Hz]; (g) Tu = 2.97%, Λ_u = 15.4mm [255 - 295 Hz];

between LST N-factor envelopes and experiments in configurations subjected to moderate levels of Tu (1.3% < Tu < 2.97%) can be explained by these free-stream turbulence levels being effective in exiting TS-waves in the pre-separated shear layer. At these moderate Tu levels, the non-linear distortion of the mean flow due to the streaks does not impact their amplification, resulting in the Orr-Sommerfeld equation predicting the correct N-factor envelopes. At a high enough Tu threshold, the mean flow modification due to the presence of streaks is too significant, resulting in the growth of wave-like disturbances being inhibited and the divergence from LST and experiment.

Consequently, using the analysis employed by Yarusevych & Kotsonis (2017), Kurelek *et al.* (2018) and Kurelek (2021), the current results show that LST is capable of modelling the convective growth of disturbances in a bubble subjected to moderate freestream turbulence levels. The critical difference is that forcing with elevated levels of FST (Tu > 1%) can cause the generation of streaks, considered to be a convective non-modal amplification of disturbances (Matsubara & Alfredsson 2001; Fransson *et al.* 2005; Fransson & Shahinfar 2020). The disturbance profiles just before and after separation presented in Fig. 19 (non-modal) strongly suggest the existence of the non-modal growth or streaks (Klebanoff modes) as the profiles exhibit self-similar behaviour with the optimal disturbance profiles from the theoretical work of Andersson *et al.* (1999) and Luchini (2000), with the maximum value of u_{rms} occurring near y/δ_1 = 1.3 for all configurations with Tu > 1%. The current results demonstrate the self-similarity of the disturbance profiles over most of the boundary layer (cf. bottom Fig. 19). Outside the boundary layer, results do not tend to zero since freestream turbulence is present, in contrast to theory, which has no freestream disturbances outside the boundary layer. Furthermore, inside the LSB, the disturbance profiles also appear to

agree well with theory. The slight downwards shift of the profile at the most advanced chordwise positions is due to the flow finishing the transition process. These observations made in Figs.18 and 19 (bottom row, non-modal) implies the co-existence of both modal and non-modal instability mechanisms, confirming the observations made by Hosseinverdi & Fasel (2019) in DNS investigations on LSBs subjected to FST and the experimental results of Veerasamy *et al.* (2021) for an attached boundary layer developing over a flat plate. In contrast, in configurations where the $Tu < 1\%$ (refer to Fig. 19, top row, modal), wall-normal disturbance profiles do not agree with theoretical predictions and do not exhibit the same behaviour as for configurations with $Tu > 1\%$, with the maxima of the peaks being between $y/\delta_1 = 0.3 - 0.5$, inferring that there is no formation of streaks and that only a viscous modal transition mechanism is present. The observation of damping behaviour on the disturbance growth presented in the previous section (Fig. 13) being due to the non-modal amplification of streaks is supported by the results in Fig. 19. The damping of disturbance growth in the bubble is also reflected in the LST predictions, as values of amplification are slightly lower for configurations subjected to elevated levels of FST, in line with what has been observed for laminar separation bubbles subjected to other methods of forcing (Marxen & Henningson 2011; Marxen *et al.* 2015; Yarusevych & Kotsonis 2017; Kurelek *et al.* 2018). Finally, it is important to note that a more rigorous characterisation could be made with the presence of spanwise hotwire measurements, however, was not possible due to the experimental setup. Nevertheless, the claim of the presence of streaks is valid based on the disturbance profiles cf. Fig. 19), decreased energy growth rates (cf. Fig. 13) and observations from previous work.

Since the height of the bubble is a relevant parameter for its stability, relating the integral parameters and the maximum growth rate can give further insights. Fig. 20 compares the variation of the non-dimensional maximum growth rate (scaled by δ_1) with the shape factor, compared with data from past studies involving laminar separation bubbles on different aerofoils. A clear relationship between the shape factor and amplification rate is present. The displacement thickness as a reference length scale effectively collapses the data on a linear trend, confirming the observations by Yarusevych & Kotsonis (2017). Although all the data in Fig. 20 are from an LSB, the experimental conditions varied substantially in the compared data sets. Experiments by Boutilier & Yarusevych (2012) fixed the Reynolds number and varied the angle of attack, while LeBlanc *et al.* (1989) varied both parameters. Yarusevych & Kotsonis (2017) studied a bubble subjected to periodic disturbances generated by a plasma actuator at a fixed Reynolds number and angle of attack. This observation implies that, for a given geometry and freestream turbulence condition, the shape factor effectively governs the non-dimensional stability characteristics of the separated shear layer. Although there are deviations between the linear trends for each data set, there is an apparent increase in the growth rate with the shape factor for different geometries and flow configurations. The proposed functional dependence on the stability characteristics extends to when the bubble is subjected to moderate levels of freestream turbulence, implying that this dependence is present even when there is a co-existence of more than one instability. In general, for a given chordwise position, as the freestream turbulence level decreases, the value of H decreases, which results in the stabilisation of the modal instability due to the increased importance of viscosity.

Finally, when the bubble is subjected to a sufficient level of freestream turbulence forcing ($Tu > 3\%$, in the present configuration), the formation of an LSB is not observed in the experimental data, suggesting that there is a critical initial forcing amplitude which will generate streaks containing enough energy to suppress boundary layer separation by promoting earlier transition. Figure. 21 confirms the existence of non-modal instabilities growing in the streamwise direction for the values of Tu where no separation was observed. Streamwise velocity disturbance profiles are in very good agreement with Andersson *et al.*

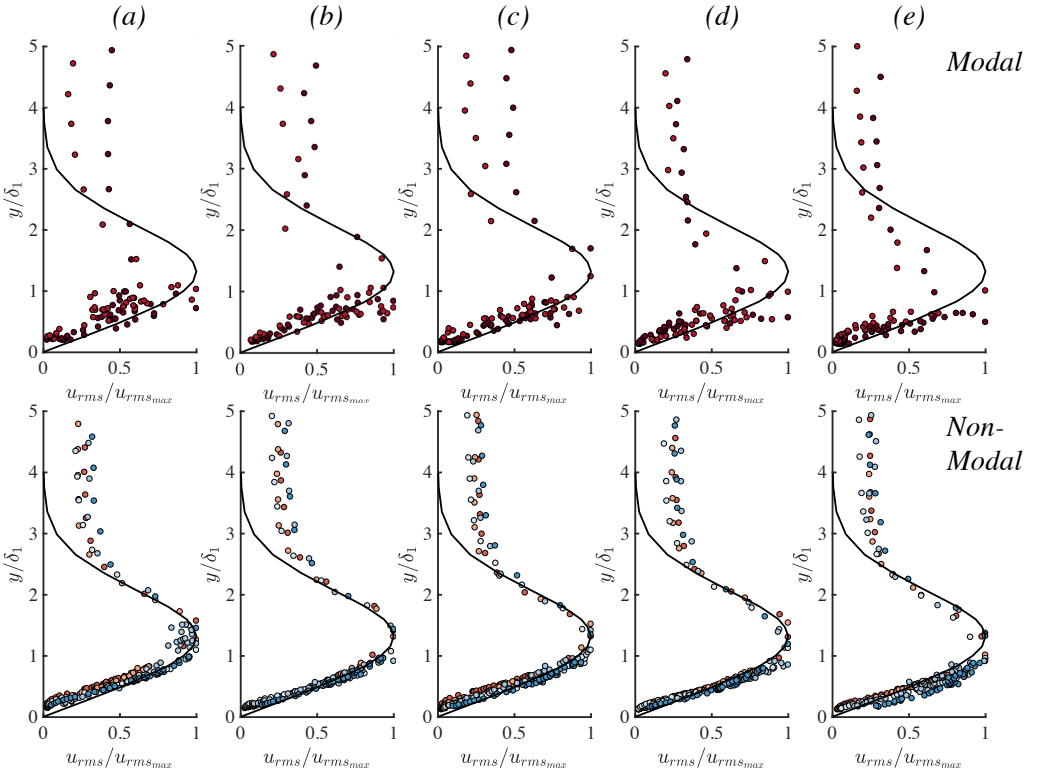

Figure 19: Streamwise velocity disturbance profiles for configurations where laminar separation bubble is subjected to turbulence of $Tu < 1\%$ (Top Row) and $Tu > 1\%$ (Bottom Row) for chordwise positions of (a) 0.325c (b) 0.350c (c) 0.375c (d) 0.400c and (e) 0.425c. Configurations with $Tu < 1\%$: NG and C0 and $Tu > 1\%$:C1-C5. Refer to Table 2 for symbols.

(1999), and Luchini (2000) exhibiting a clear peak at $y/\delta_1 \approx 1.3$, with profiles further downstream manifesting a lower wall-normal position of the maxima due to the flow undergoing transition and tending to a turbulent state where the peak in the fluctuating velocity component is closer to the wall. Furthermore, the u_{rms} profiles exhibit no peaks below $y/\delta_1 \approx 1.3$, in stark contrast to what is observed in configurations containing a laminar separation bubble. At the highest levels of freestream turbulence, the bubble could be suppressed due to the boundary layer transitioning before the ideal separation point. Another possibility of the suppression of the LSB (at least for the current experimental configuration) could be due to the presence of streaks in the boundary layer, which were recently observed in a numerical investigation by Xu & Wu (2021). They found freestream vortical disturbances of moderate level prevent the separation in a boundary layer flow over a plate or concave wall, inferring that the strong nonlinear mean-flow distortion associated with the nonlinear streaks or Görtler vortices prevents separation. In our experiments, the suppression of laminar separation could be due to critically energetic streaks caused by sufficiently elevated freestream turbulence levels.

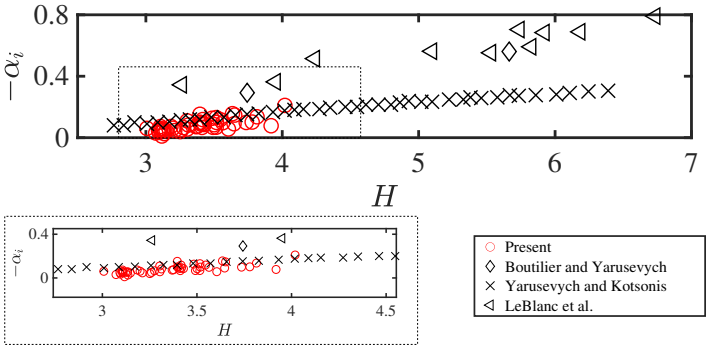

Figure 20: Maximum growth rate as a function of the LSB shape factor for all tested configurations.

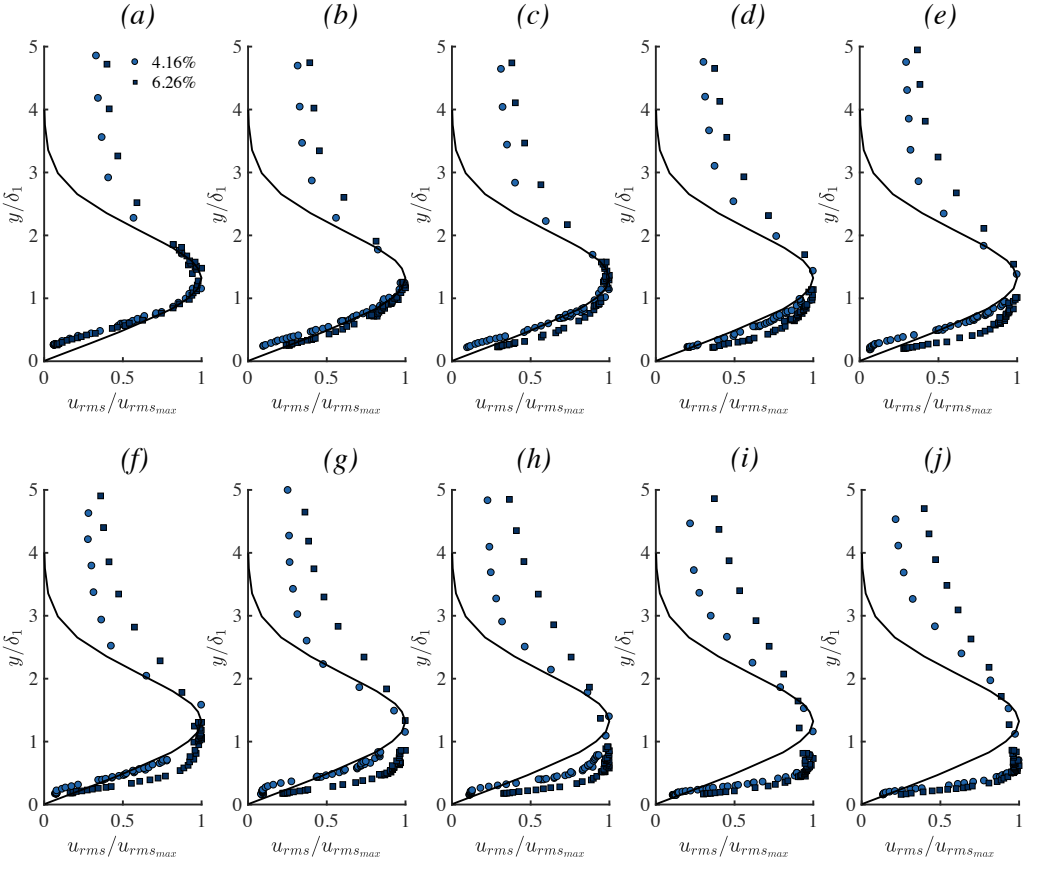

Figure 21: Chordwise evolution of the disturbance profiles scaled with $u_{rms,max}$ for chordwise positions of (a) 0.250c (b) 0.300c (c) 0.325c (d) 0.350c (e) 0.375c (f) 0.400c (g) 0.425c (h) 0.450c (i) 0.475c (j) 0.500c . Black line denoted theoretical optimal perturbation profile by Luchini (2000). Configurations C6 and C7: Refer to Table 2 for symbols.

4. Concluding Remarks

The present investigation examines the effects of varying the freestream turbulence intensity and integral length scale on the flow development and transition in a laminar separation bubble. The laminar separation bubble develops over the suction side of a NACA0015 aerofoil at a chord based Reynolds number of 125000 and angle of incidence of 2.3° in a low freestream turbulence open circuit wind tunnel. Freestream turbulence was generated in a controlled manner using regular and fractal grids resulting in a wide range of levels of turbulence intensity and integral length scales. The streamwise evolution of freestream turbulence and the flow field were characterised using hotwire anemometery, with the spanwise homogeneity of the flow field being verified with infra-red thermography. In total, 8 freestream flow configurations were tested, three with a fixed level of turbulence intensity, but variable integral length scale. The results exhibit that, elevated levels of freestream turbulence, reduce the size of the mean bubble flow topology, advancing the transition position, decreasing the size of the bubble, with its eventual elimination at the highest levels, in accordance with previous investigations in the literature. In the laminar separation bubble, the convective development of an unstable frequency band is observed and is broadened with the addition of freestream turbulence, a consequence of more significant energy content within a broader range of frequencies from the freestream turbulence. The presence of freestream turbulence also shifts the most amplified frequency band to a higher spectral range, due to a smaller wall normal and streamwise length of the bubble when excited. In the baseline case, when the most amplified frequencies are non-dimensionlised through the use of a Strouhal number based on the boundary layer momentum thickness at separation, St_{δ_2}, agreement is found with Pauley *et al.* (1990). However, increasing the Tu causes St_{δ_2} to increase, when compared to the baseline case, and approach values closer to what was proposed by Rodríguez *et al.* (2021), however, but increases consistently with an increase in Tu.

The present investigation examines the effects of varying the freestream turbulence intensity and integral length scale on the flow development and transition in a laminar separation bubble. The laminar separation bubble develops over the suction side of a NACA0015 aerofoil at a chord-based Reynolds number of 125000 and angle of incidence of 2.3° in a low freestream turbulence open circuit wind tunnel. Freestream turbulence was generated in a controlled manner using regular and fractal grids resulting in a wide range of levels of turbulence intensity and integral length scales. The streamwise evolution of freestream turbulence and the flow field were characterised using hotwire anemometry. Eight freestream flow configurations were tested, three with a fixed turbulence intensity level but a variable integral length scale.

The results exhibit that elevated levels of freestream turbulence reduce the size of the mean bubble flow topology, advancing the transition position, and decreasing the size of the bubble, with its eventual elimination at the highest levels, following previous investigations in the literature. In the laminar separation bubble, the convective development of an unstable frequency band is observed and is broadened with the addition of freestream turbulence, a consequence of more significant energy content within a broader range of frequencies from the freestream turbulence. The presence of freestream turbulence also shifts the most amplified frequency band to a higher spectral range due to a smaller wall-normal and streamwise length of the bubble when excited. In the baseline case, when the most amplified frequencies are non-dimensionlised through the use of a Strouhal number based on the boundary layer momentum thickness at separation, St_{δ_2}, an agreement is found with Pauley *et al.* (1990). However, increasing the Tu causes St_{δ_2} to increase when compared to the baseline case, and approach values closer to what was proposed by Rodríguez *et al.* (2021), however, but increases consistently with an increase in Tu.

The presence of streaks is observed for configurations with $Tu > 1\%$, with unfiltered profiles agreeing remarkably well with the theoretical optimal perturbation profile at multiple chordwise positions before and inside the laminar separation bubble. The mechanism of disturbance energy growth gradually changes from an exponential one, at lower levels of Tu, to an algebraic one for the more extreme Tu levels, growing until the energy saturates. In the configuration where a bubble is present, band-pass filtered (corresponding to the most amplified frequency range) values of disturbance energy reveal the gradual reduction in the slope of the chordwise energy growth with increasing Tu and suggesting that the non-modal instabilities become more dominant, which can be thought of as competing with the modal instabilities. Once the turbulence forcing reaches a critical level, $Tu \approx 4\%$ in the present case, the streaks in the boundary layer are too energetic to allow the flow to separate, ensuing in the elimination of the modal instability via the non-modal instability and suppressing the formation of the bubble. The damping of the streamwise growth of disturbances is due to the presence of streaks (Klebanoff modes) caused by the elevated levels of freestream turbulence, which change the mean flow topology of the bubble through the introduction of non-modal disturbances into the boundary layer. Finally, for a relatively fixed level of Tu, the variation of Λ_u has modest effects; however, a slight advancement of transition with the decrease in Λ_u is observed and has been reported in previous work.

Local linear stability analysis is shown to accurately model incipient distance growth for the unexcited turbulence case, in agreement with previous work (Yarusevych & Kotsonis 2017; Kurelek *et al.* 2018; Kurelek 2021). Moreover, good agreement between LST eigenfunctions and filtered experimental u_{rms} profiles and prediction of the most amplified frequencies is found. In the presence of elevated turbulence, LST predicts the growth of disturbances and unstable frequencies with acceptable accuracy. Counterintuitively, an augmented agreement between experiment and LST for N-factor envelopes was present in configurations subjected to moderate levels of FST and was thought to be due to the turbulence being effective in exiting the viscous modal instabilities in the pre-separated shear-layer. Additionally, filtered u_{rms} profiles were representative of those predicted by LST and resembled those which are expected in the presence of modal visco-inflectional instabilities. The current work provides rigorous experimental evidence on the co-existence of modal and non-modal instabilities in a laminar separation bubble, which has been observed in recent direct numerical simulations of Hosseinverdi & Fasel (2019). Further insights on the characteristics of the modal instability were obtained. At low Tu, a larger range of unstable frequencies was present due to the inflectional point being further away from the wall than configurations subjected to elevated turbulence levels. A clear relationship between the shape factor and amplification rate was present, such that a decrease in the shape factor results in the stabilisation of the modal instability due to the increased importance of viscosity. The proposed functional dependence on the stability characteristics extends to when the bubble is subjected to moderate levels of freestream turbulence, implying that this dependence is present even when there is a co-existence of more than one instability.

REFERENCES

Andersson, Paul, Berggren, Martin & Henningson, Dan S 1999 Optimal disturbances and bypass transition in boundary layers. *Physics of Fluids* **11** (1), 134–150.

Arnal, D & Julien, JC 1978 Contribution expérimentale à l'etude de la receptivité d'une couche limite laminaire, à la turbulence de l'écoulement generale. *Rapport Technique 1/5018 AYD* .

Balzer, Wolfgang & Fasel, Hermann 2016 Numerical investigation of the role of free-stream turbulence in boundary-layer separation. *Journal of Fluid Mechanics* **801**, 289–321.

Benedict, LH & Gould, RD 1996 Towards better uncertainty estimates for turbulence statistics. *Experiments in Fluids* **22** (2), 129–136.

946 Boutilier, Michael SH & Yarusevych, Serhiy 2012 Separated shear layer transition over an airfoil at a
947 low Reynolds number. *Physics of Fluids* **24** (8), 084105.
948 Boutilier, Michael SH & Yarusevych, Serhiy 2013 Sensitivity of linear stability analysis of measured
949 separated shear layers. *European Journal of Mechanics-B/Fluids* **37**, 129–142.
950 Boutilier, Michael Stephen Hatcher 2011 Experimental investigation of transition over a NACA 0018
951 airfoil at a low Reynolds number. Master's thesis, University of Waterloo.
952 Brandt, Luca, Schlatter, Philipp & Henningson, Dan S 2004 Transition in boundary layers subject to
953 free-stream turbulence. *Journal of Fluid Mechanics* **517**, 167.
954 Breuer, Michael 2018 Effect of inflow turbulence on an airfoil flow with laminar separation bubble: An
955 LES study. *Flow, Turbulence and Combustion* **101** (2), 433–456.
956 Bridges, TJ & Morris, Philip John 1984 Differential eigenvalue problems in which the parameter appears
957 nonlinearly. *Journal of Computational Physics* **55** (3), 437–460.
958 Bruun, Hans H 1996 Hot-wire anemometry: principles and signal analysis.
959 Burattini, Paolo & Antonia, Robert A 2005 The effect of different X-wire calibration schemes on some
960 turbulence statistics. *Experiments in Fluids* **38** (1), 80–89.
961 Burgmann, Sebastian & Schröder, W 2008 Investigation of the vortex induced unsteadiness of a
962 separation bubble via time-resolved and scanning PIV measurements. *Experiments in Fluids* **45** (4),
963 675–691.
964 Carmichael, BH 1981 Low Reynolds number airfoil survey, volume 1. *NASA 165803* **1**.
965 Cherubini, Stefania, Robinet, J-Ch, De Palma, Pietro & Alizard, Frédéric 2010 The onset of three-
966 dimensional centrifugal global modes and their nonlinear development in a recirculating flow over a
967 flat surface. *Physics of Fluids* **22** (11), 114102.
968 Dellacasagrande, Matteo, Barsi, Dario, Lengani, Davide, Simoni, Daniele & Verdoya, Jacopo
969 2020 Response of a flat plate laminar separation bubble to Reynolds number, free-stream turbulence
970 and adverse pressure gradient variation. *Experiments in Fluids* **61** (6).
971 Diwan, Sourabh S & Ramesh, ON 2009 On the origin of the inflectional instability of a laminar separation
972 bubble. *Journal of Fluid Mechanics* **629**, 263–298.
973 Dovgal, AV, Kozlov, VV & Michalke, A 1994 Laminar boundary layer separation: instability and
974 associated phenomena. *Progress in Aerospace Sciences* **30** (1), 61–94.
975 Drela, Mark 1989 XFOIL: An analysis and design system for low Reynolds number airfoils. In *Low*
976 *Reynolds number aerodynamics*, pp. 1–12. Springer.
977 Fransson, Jens HM, Matsubara, Masaharu & Alfredsson, P Henrik 2005 Transition induced by
978 free-stream turbulence. *Journal of Fluid Mechanics* **527**, 1–25.
979 Fransson, Jens HM & Shahinfar, Shahab 2020 On the effect of free-stream turbulence on boundary-layer
980 transition. *Journal of Fluid Mechanics* **899**.
981 Gaster, M 1967 *The structure and behaviour of laminar separation bubbles*, , vol. RM 3595. Aeronaut.Res.
982 Counc.
983 Häggmark, CP, Bakchinov, Andrey A & Alfredsson, P Henrik 2000 Experiments on a two–dimensional
984 laminar separation bubble. *Philosophical Transactions of the Royal Society of London. Series A:*
985 *Mathematical, Physical and Engineering Sciences* **358** (1777), 3193–3205.
986 Häggmark, Carl P, Hildings, C & Henningson, Dan S 2001 A numerical and experimental study of a
987 transitional separation bubble. *Aerospace Science and Technology* **5** (5), 317–328.
988 Hislop, George Steedman 1940 The transition of a laminar boundary layer in a wind tunnel. PhD thesis.
989 Hosseinverdi, Shirzad 2014 Influence of free-stream turbulence on laminar-turbulent transition in long
990 laminar separation bubbles: Direct Numerical Simulations. Master's thesis.
991 Hosseinverdi, Shirzad & Fasel, Hermann 2019 Numerical investigation of laminar–turbulent transition
992 in laminar separation bubbles: the effect of free-stream turbulence. *Journal of Fluid Mechanics* **858**,
993 714–759.
994 Houdeville, R 1992 Three-dimensional boundary layer calculation by a characteristic method. In *Fifth*
995 *Symposium on Numerical and Physical Aspects of Aerodynamic Flows, Long Beach, January 1992*.
996 Hurst, D & Vassilicos, JC 2007 Scalings and decay of fractal-generated turbulence. *Physics of Fluids*
997 **19** (3), 035103.
998 Istvan, Mark S & Yarusevych, Serhiy 2018 Effects of free-stream turbulence intensity on transition in
999 a laminar separation bubble formed over an airfoil. *Experiments in Fluids* **59** (3), 52.
1000 Jaroslawski, Thomas, Forte, Maxime, Moschetta, Jean-Marc, Delattre, Gregory & Gowree,
1001 Erwin R 2022 Characterisation of boundary layer transition over a low Reynolds number rotor.
1002 *Experimental Thermal and Fluid Science* **130**, 110485.

Jonáš, Pavel, Mazur, Oton & Uruba, Václav 2000 On the receptivity of the by-pass transition to the length scale of the outer stream turbulence. *European Journal of Mechanics-B/Fluids* **19** (5), 707–722.

Jones, LE, Sandberg, RD & Sandham, ND 2010 Stability and receptivity characteristics of a laminar separation bubble on an aerofoil. *Journal of Fluid Mechanics* **648**, 257–296.

Kendall, James 1998 Experiments on boundary-layer receptivity to freestream turbulence. In *36th AIAA Aerospace Sciences Meeting and Exhibit*, p. 530.

Klebanoff, PS & Tidstrom, KD 1972 Mechanism by which a two-dimensional roughness element induces boundary-layer transition. *Physics of Fluids* **15** (7), 1173–1188.

Kurelek, John 2021 The vortex dynamics of laminar separation bubbles. PhD thesis, University of Waterloo.

Kurelek, John William, Kotsonis, Marios & Yarusevych, Serhiy 2018 Transition in a separation bubble under tonal and broadband acoustic excitation. *Journal of Fluid Mechanics* **853**, 1–36.

Kurelek, John W, Lambert, Andrew R & Yarusevych, Serhiy 2016 Coherent structures in the transition process of a laminar separation bubble. *AIAA Journal* **54** (8), 2295–2309.

Kurian, Thomas & Fransson, Jens HM 2009 Grid-generated turbulence revisited. *Fluid dynamics research* **41** (2), 021403.

LeBlanc, P, Blackwelder, R & Liebeck, R 1989 A comparison between boundary layer measurements in a laminar separation bubble flow and linear stability theory calculations. In *Low Reynolds Number Aerodynamics*, pp. 189–205. Springer.

Li, Hua J & Yang, Zhiyin 2019 Separated boundary layer transition under pressure gradient in the presence of free-stream turbulence. *Physics of Fluids* **31** (10), 104106.

Luchini, Paolo 2000 Reynolds-number-independent instability of the boundary layer over a flat surface: optimal perturbations. *Journal of Fluid Mechanics* **404**, 289–309.

Lueptow, RM, Breuer, KS & Haritonidis, JH 2004 Computer-aided calibration of X-probes using a look-up table. *Experiments in Fluids* **6** (2), 115–118.

Makita, H & Sassa, K 1991 Active turbulence generation in a laboratory wind tunnel. In *Advances in turbulence 3*, pp. 497–505. Springer.

Mamidala, Santhosh B, Weingärtner, André & Fransson, JHM 2022 Leading-edge pressure gradient effect on boundary layer receptivity to free-stream turbulence. *Journal of Fluid Mechanics* **935**.

Marxen, Olaf & Henningson, Dan S 2011 The effect of small-amplitude convective disturbances on the size and bursting of a laminar separation bubble. *Journal of Fluid Mechanics* **671**, 1–33.

Marxen, Olaf, Kotapati, Rupesh B, Mittal, Rajat & Zaki, Tamer 2015 Stability analysis of separated flows subject to control by zero-net-mass-flux jet. *Physics of Fluids* **27** (2), 024107.

Marxen, O, Lang, M, Rist, U & Wagner, S 2003 A combined experimental/numerical study of unsteady phenomena in a laminar separation bubble. *Flow, Turbulence and Combustion* **71** (1-4), 133–146.

Matsubara, M & Alfredsson, P Henrik 2001 Disturbance growth in boundary layers subjected to free-stream turbulence. *Journal of Fluid Mechanics* **430**, 149.

Methel, Jeanne, Forte, Maxime, Vermeersch, Olivier & Casalis, Grégoire 2019 An experimental study on the effects of two-dimensional positive surface defects on the laminar–turbulent transition of a sucked boundary layer. *Experiments in Fluids* **60** (6), 1–18.

Michelis, Theodoros, Yarusevych, Serhiy & Kotsonis, Marios 2017 Response of a laminar separation bubble to impulsive forcing. *J. Fluid Mech* **820**, 633–666.

Morkovin, Mark V 1985 Bypass transition to turbulence and research desiderata. *Transition in Turbines* **2386**, 161–204.

Nolan, KP, Walsh, EJ & McEligot, DM 2010 Quadrant analysis of a transitional boundary layer subject to free-stream turbulence. *Journal of Fluid Mechanics* **658**, 310.

Olson, David A, Katz, Alan W, Naguib, Ahmed M, Koochesfahani, Manoochehr M, Rizzetta, Donald P & Visbal, Miguel R 2013 On the challenges in experimental characterization of flow separation over airfoils at low Reynolds number. *Experiments in Fluids* **54** (2), 1–11.

Ovchinnikov, Victor, Choudhari, Meelan M & Piomelli, Ugo 2008 Numerical simulations of boundary-layer bypass transition due to high-amplitude free-stream turbulence. *Journal of Fluid Mechanics* **613**, 135–169.

Pauley, Laura L 1994 Structure of local pressure-driven three-dimensional transient boundary-layer separation. *AIAA Journal* **32** (5), 997–1005.

Pauley, Laura L, Moin, Parviz & Reynolds, William C 1990 The structure of two-dimensional separation. *Journal of Fluid Mechanics* **220**, 397–411.

Rist, Ulrich & Maucher, Ulrich 2002 Investigations of time-growing instabilities in laminar separation bubbles. *European Journal of Mechanics-B/Fluids* **21** (5), 495–509.

Rodríguez, D & Gennaro, EM 2019 Enhancement of disturbance wave amplification due to the intrinsic three-dimensionalisation of laminar separation bubbles. *The Aeronautical Journal* **123** (1268), 1492–1507.

Rodríguez, Daniel, Gennaro, Elmer M & Souza, Leandro F 2021 Self-excited primary and secondary instability of laminar separation bubbles. *Journal of Fluid Mechanics* **906**.

Rodriguez, Daniel & Theofilis, Vassilis 2010 Structural changes of laminar separation bubbles induced by global linear instability. *Journal of Fluid Mechanics* **655**, 280–305.

Schmid, Peter J & Henningson, Dan S 2000 *Stability and transition in shear flows*, , vol. 142. Springer Science & Business Media.

Serna, J & Lázaro, BJ 2014 The final stages of transition and the reattachment region in transitional separation bubbles. *Experiments in Fluids* **55** (4), 1–17.

Simoni, Daniele, Lengani, Davide, Ubaldi, Marina, Zunino, Pietro & Dellacasagrande, Matteo 2017 Inspection of the dynamic properties of laminar separation bubbles: free-stream turbulence intensity effects for different Reynolds numbers. *Experiments in Fluids* **58** (6), 66.

Studer, G, Arnal, D, Houdeville, R & Seraudie, A 2006 Laminar–turbulent transition in oscillating boundary layer: experimental and numerical analysis using continuous wavelet transform. *Experiments in Fluids* **41** (5), 685–698.

Veerasamy, Dhamotharan, Atkin, Chris J & Ponnusami, Sathiskumar A 2021 Aerofoil wake-induced transition characteristics on a flat-plate boundary layer. *Journal of Fluid Mechanics* **920**.

Volino, Ralph J 1997 A new model for free-stream turbulence effects on boundary layers. In *Turbo Expo: Power for Land, Sea, and Air*, , vol. 78705, p. V003T09A015. American Society of Mechanical Engineers.

Watmuff, Jonathan H 1999 Evolution of a wave packet into vortex loops in a laminar separation bubble. *Journal of Fluid Mechanics* **397**, 119–169.

Westin, KJA, Boiko, AV, Klingmann, BGB, Kozlov, VV & Alfredsson, PH 1993 Experiments in a boundary layer subjected to free stream turbulence. Part 1: Boundary layer structure and receptivity. *Tech. Rep.*. Royal Inst. of Tech.

Wissink, JG & Rodi, W 2006 Direct Numerical Simulations of transitional flow in turbomachinery. *Journal of Turbomachinery* **128** (4), 668–667.

Xu, Dongdong & Wu, Xuesong 2021 Elevated low-frequency free-stream vortical disturbances eliminate boundary-layer separation. *Journal of Fluid Mechanics* **920**.

Xu, Hui, Mughal, Shahid M, Gowree, Erwin R, Atkin, Chris J & Sherwin, Spencer J 2017 Destabilisation and modification of tollmien–schlichting disturbances by a three-dimensional surface indentation. *Journal of Fluid Mechanics* **819**, 592–620.

Yarusevych, Serhiy & Kotsonis, Marios 2017 Steady and transient response of a laminar separation bubble to controlled disturbances. *Journal of Fluid Mechanics* **813**, 955–990.

Zaman, KBMQ, McKinzie, DJ & Rumsey, CL 1989 A natural low-frequency oscillation of the flow over an airfoil near stalling conditions. *Journal of Fluid Mechanics* **202**, 403–442.